DIAGNOSIS OF FRACTURE FLOW CONDITIONS WITH ACOUSTIC SENSING

A Thesis

by

ROBERTO MARTINEZ JR.

Submitted to the Office of Graduate and Professional Studies of
Texas A&M University
in partial fulfillment of the requirements for the degree of

MASTER OF SCIENCE

Chair of Committee,	Alfred Daniel Hill
Co-Chair of Committee,	Ding Zhu
Committee Member,	Yong-Joe Kim
Head of Department,	Alfred Daniel Hill

August 2014

Major Subject: Petroleum Engineering

Copyright 2014 Roberto Martinez Jr.

ABSTRACT

Distributed acoustic sensing (DAS) is an emerging technology in hydraulic fracture diagnosis. Current uses of DAS systems have been limited to qualitative analysis that pinpoint noise sources, such as injection into formation or production from a fracture. Identification of noise verifies that injection or production is happening and its sound intensities at the different locations give a relative indication as to which locations took more fluid or produced more fluid post-treatment.

Signal processing techniques and quantitative analysis are used to measure flow rates in a simulated fractured well. Production into a 5-½ inch OD well was simulated by injecting fluid through packed bed of 16/30 mesh, 20/40 mesh and 30/50 mesh proppant. Gas was injected at varying rates into the fracture and into the well. The noise produced from production was recorded with a hydrophone. The acoustic signal was transformed from the time domain to the frequency domain through a fast Fourier transform (FFT) for analysis.

The experimental results showed that the frequency of sound and its intensity were crucial in determining the amount of fluid being produced. The sound level of the peak frequencies were found to be linearly related to the flow rate. The results verified that sound alone can be used to measure flow rate through a proppant packed fracture and perforation tunnel. Incorporation of this technique into current DAS systems can give a real time value for injection rates during hydraulic fracture treatments and for production rates from post treatment measurements.

DEDICATION

I dedicate this to my mother and father.

ACKNOWLEDGEMENTS

My gratitude goes to Dr. Hill and Dr. Zhu for giving me the opportunity to conduct research under their supervision and guidance. I am also thankful to Dr. Kim, for his guidance on acoustic topics.

Thank you to my office mates who made my stay at Texas A&M memorable, Dare, Jingyuan, Nozomu, Rudy, Xinyang and ZJ.

NOMENCLATURE

a_o	Speed of sound
F_s	Sampling frequency (Hz)
$H(f)$	Heavyside function
L	15 cm
n	Index
M	Mach number
M_i	Local source Mach number vector
N_{Re}	Reynolds number
p	Pressure
P_{ij}	Compressive stress tensor
p'	Acoustic pressure
p'_T	Thickness term
p'_L	Loading term
r	Distance to observer
t	Time
T	Sampling period (seconds)
T_{ij}	Lighthill stress tensor
V	Mean fluid velocity
u_i	Fluid velocity

u_n	Fluid velocity components normal to surface
v_i	Fluid velocity
v_n	Fluid velocity components normal to surface
$x(n)$	Discrete time signal
$x(t)$	Continuous signal
$X(\omega)$	Fourier transform

Greek

$\delta(f)$	Dirac delta function
μ	Fluid viscosity
ρ	Fluid density
τ_{ij}	Subgrid-scale stress term
ω	Radial frequency
ω_{c1}	Low frequency cut off
ω_{c2}	High frequency cut off

TABLE OF CONTENTS

Page

Page

LIST OF FIGURES

Page

Page

Page

LIST OF TABLES

Page

1. INTRODUCTION*

1.1 Background

Due to recent interest in developing petroleum fluids from unconventional shale resources, much attention has been focused on hydraulic fracturing as a means of increasing the productivity of low permeability formations. The objective of hydraulic fracturing is to induce fractures in the formation.

In shale, it is common to drill horizontal wells with transverse fractures. During the fracturing process, the amount of fluid injected into the formation is known, however determining where exactly fracturing fluid is injected has been a difficult task with conventional tools.

Advances in fracture diagnosis have enabled engineers to monitor where fluid is being injected. This monitoring is done through implementation of fiber optic technology. With fiber optic technology engineers monitor the temperature and sound intensity along the length of the wellbore. With changes in temperature and sound intensity it is possible to identify at what depth or length along the wellbore, fluid is being injected. These sensing systems are known as distributed acoustic sensing (DAS) and distributed temperature sensing (DTS) systems.

---

* Part of this thesis is reprinted with permission from "Diagnosis of Flow Conditions from Fractures with Acoustic Sensing" by R. Martinez, A.D. Hill, and D. Zhu. Paper SPE 168601 presented at the SPE Hydraulic Fracturing Technology Conference in the Woodlands, Texas, U.S.A., 4-6 February 2014. Copyright 2014 by the Society of Petroleum Engineers.

Post-fracture treatment, DAS data can be used to identify where fluid is being produced from fractures. In addition, because sound is recorded along the entire length of the well, a comparison of this sound across zones gives an indication of the zones or fractures that produce the most and those that produce the least.

1.2 Literature Review

1.2.1 Noise Logging

The idea of using sound for well diagnosis, termed noise logging, started in 1955 with efforts from Enright (1955)**.** It wasn't until 1973 however, that acoustic logging became commercially viable based on research by McKinley et al. (1973). By recording sound at multiple points within the well a noise log is created. The sound recorded at these multiple points gives an indication of where fluid movement occurs as the sound is created by fluid turbulence. The high amplitude sounds indicate flow through a channel, leaks, flow from perforations and flow past the logging sonde (McKinley et al. 1973).

Noise logging started as a qualitative tool to determine where leaks and fluid movement occur in a well, however, experiments by McKinley et al. (1973) demonstrated that noise logging could be used as a quantitative tool. The work of McKinley et al. sought to find a relationship between flow rates and the amplitude of the peak noise observed from his experiments. McKinley et al. throttled fluid through channels to simulate leaking and to simulate production from an orifice. An example of noise spectra for fluid throttling across a perforation at various pressure gradients are shown in **Fig. 1**.

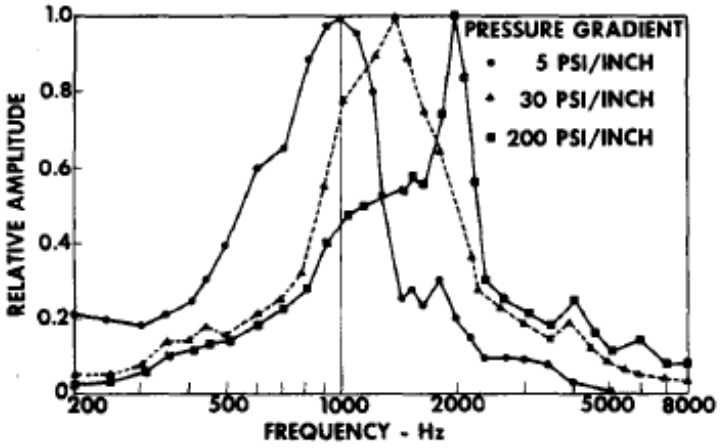

Fig. 1 Sound Spectrum for Water Throttling Across Different Pressure Gradient (McKinley et al. 1973)

The experimental results presented by McKinley et al. in **Fig. 1** show that a dominant peak in the frequency spectrum is observed when fluid is throttled across an orifice. As explained by Hill (1990), McKinley et al. related the amplitude of the peak frequencies observed to an energy dissipation rate and found that amplitude of the peaks, a, is related to the product of pressure drop and flow rate,

$$a = f(\Delta p_t q) \quad \text{.....} \quad (1.6)$$

This correlation of noise amplitude with energy dissipation rate can be seen in **Fig 2**.

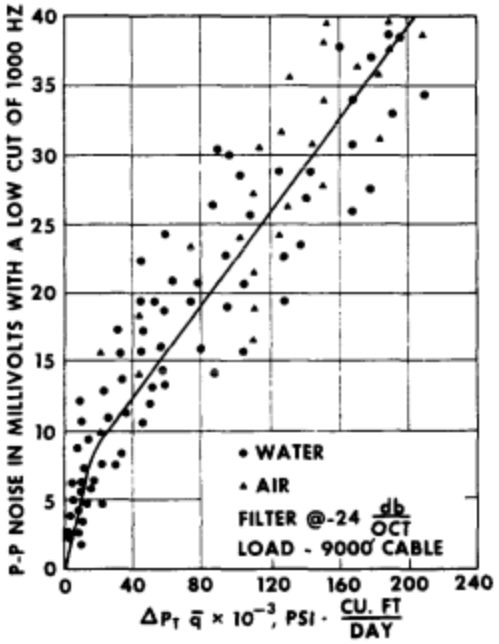

Fig. 2 Correlation of Noise Amplitude with Energy Dissipation Rate (McKinley et al. 1973)

The correlation depicted in **Fig 2** is for single-phase flow in a channel behind one string of water-filled casing (McKinley et al. 1973).

McKinley et al. implemented knowledge gained from experiments to a field case where noise logging was successfully implemented to quantify gas flow in a channel. The noise log taken in the well depicted in **Fig. 3,** confirmed that gas was flowing through a channel behind the casing.

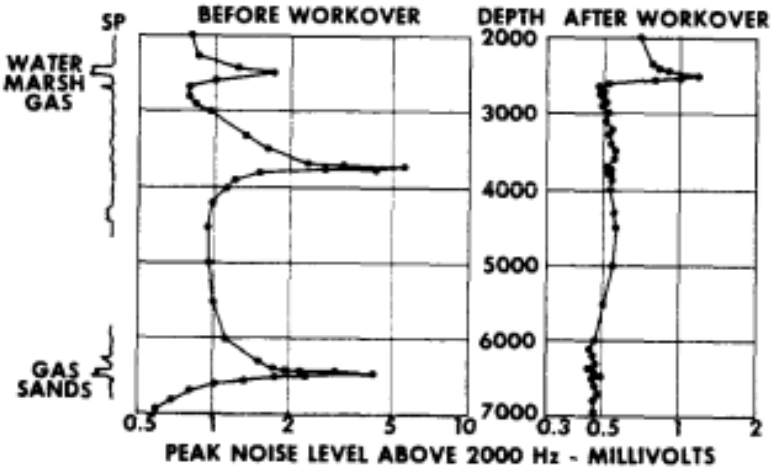

Fig. 3 Noise Logs of Tubingless Completion Leaking to Surface (McKinley et al. 1973)

By cement squeezing above and below the gas source at 6,445 ft., the gas source was eliminated. This was confirmed with a pressure drop in the annulus and with a noise log after the workover. As seen in **Fig. 3** the sound of gas is no longer detected at 3,730 and 6,455 ft. after the workover.

Robinson (1976) published noise-logging field results for a variety of wells to detect production and leaks. Robinson observed similar results to McKinley et al. in that the peak amplitude frequencies gave indication of flow rate. Despite the accomplishments by McKinley et al. and successful implementation of noise logging by Robinson, there was a lack of interest in sound as a method of determining production rates until DAS systems via fiber optic became feasible. Yet, the work that has been released to the general public does not address what improvements or advances in quantifying flow rates from sound have been made since McKinley's work.

1.2.2 Distributed Acoustic Sensing Technology

The sound that is recorded by DAS is caused by fluid vibrations inside the wellbore. As fluid vibrates, pressure waves propagate through the fluid and reach the long sensing fiber optic cable. When these pressure waves reach the fiber optic cable, they cause strain on the cable. A visualization of a DAS system is shown in **Fig. 4**.

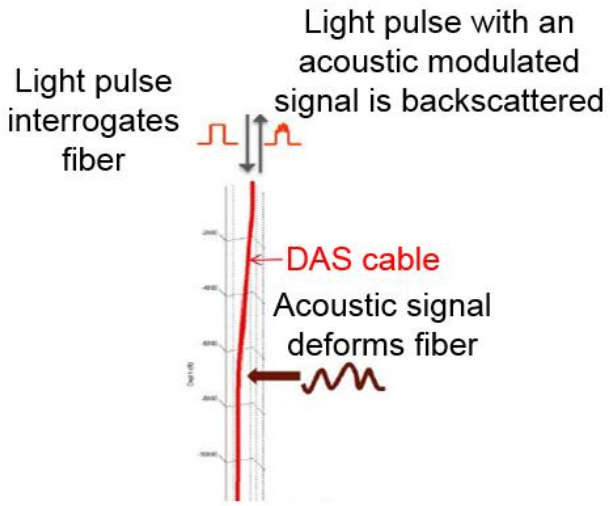

Fig. 4 Visualization of a DAS System (Mateeva et al. 2012)

This strain is quantified by the modulated light that is traveling through the fiber. A light pulse, at a known rate and intensity, is sent through the fiber optic cable, however, when this light pulse reaches an area where the cable has been deformed by the acoustic pressure waves, the manner in which this pulse travels through the fiber optic cable changes. When this modulated light pulse reaches the surface, it is backscattered, and through signal processing, this backscattered light pulse gives an indication of where

the acoustic pressure wave deformed the cable and the properties of the acoustic wave such as the frequency in Hz and the amplitude in Pascals can be determined.

The fiber optic cable consists of two concentric glass regions with different refractive indices (Ferguson 2012) as shown in **Fig. 5**. The region where the majority of the light travels through the fiber is called the core. The outer covering is the cladding which has a lower refractive index.

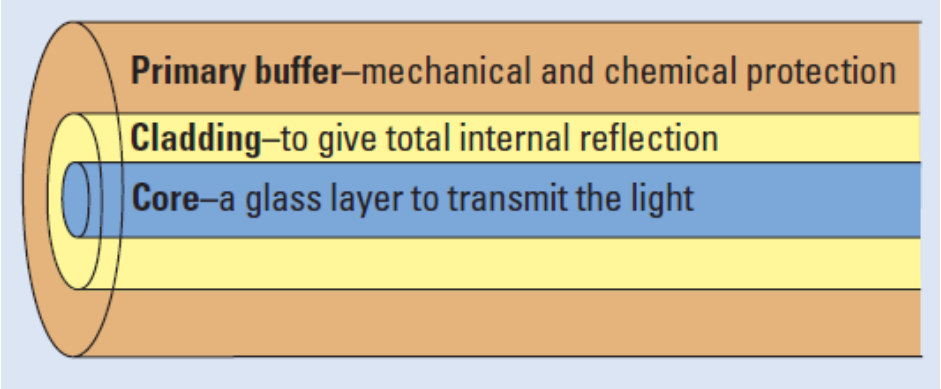

Fig. 5. Diagram of Fiber Optic Cable (Ferguson 2002)

Two different fiber optic cables are implemented: single-mode or multi-mode. In a multi-mode cable, light is reflected at the boundary between the core and cladding and as a result travels in traverse modes such as helically or in a zig-zag mode. On the other hand, in single-mode fibers, light travels down the fiber on a single axis. **Fig. 6** shows the different modes light can travel in a fiber optic cable.

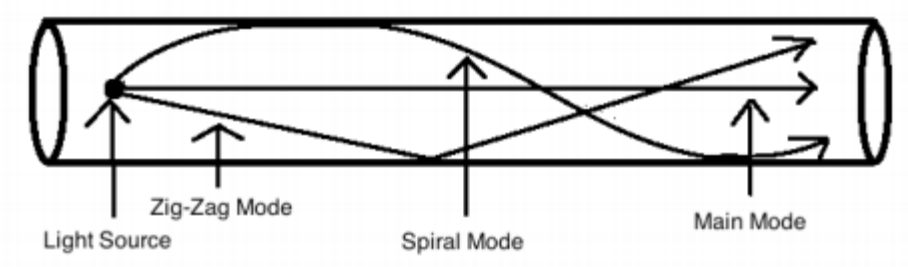

Fig. 6 Modes of Light Travel in Fiber Optic Cable (Cannon et al. 2013)

The mode in which light travels is greatly influenced by the dimensions of the fiber optic cable. A single-mode fiber has a 10 μm core diameter, restricting one mode of light to propagate through the fiber. A multi-mode fiber is larger with a core diameter of 63.5 μm that allows for multiple modes of light to propagate through the fiber (Ferguson et al. 2002). The cross section of a fiber optic cable is shown in **Fig. 7**.

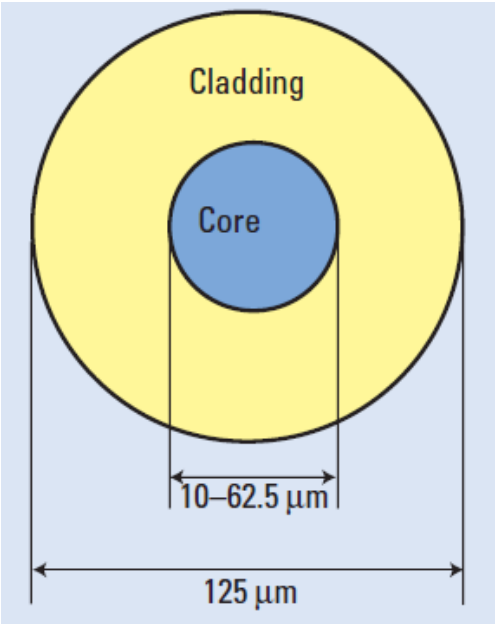

Fig. 7 Cross Section of Fiber Optic Cable (Ferguson 2002)

Another characteristic essential to DAS systems is the frequency at which light can be pulsed down the fiber, the reason being, in order to resolve signals without aliasing, a high enough pulse rate must be used. A simple method to estimate the maximum pulse rate:

$$f_{\text{max rate}} = \frac{\text{speed light travels through fiber}}{\text{total length traveled}} \quad \text{..... (1.7)}$$

$$f_{\text{max rate}} = \frac{\text{speed of light in a vacuum / refractive index of fiber}}{2\times\text{length of fiber}} \quad \text{..... (1.8)}$$

$$f_{\text{max rate}} = \frac{3\times10^{8}\ ms^{-1}/1.5}{2\times L} \quad \text{..... (1.9)}$$

$$f_{\text{max rate}} = \frac{1\times10^{8}\ ms^{-1}}{L} \quad \text{..... (1.10)}$$

If the length of the fiber is the same as the length of the well, then for a ten thousand foot well the maximum pulse rate would be 33 kHz, giving a maximum frequency response of 16.5 kHz. This means sound with frequencies up to 16.5 kHz can be detected and resolved.

This fiber optic cable that can sense acoustic pressure waves are installed along the length of the wellbore. By sending a light pulse through the fiber optic cable and analyzing modulated light pulses, engineers determine where sound events occur and determine the sound intensity. The ability to determine where sound is being generated enables engineers monitor wellbores and determine leaks; speculate where fluid is being produced from perforations or fractures and determine where fluid is being injected during hydraulic fracturing.

1.2.3 Distributed Acoustic Sensing Field Cases

Monitoring Hydraulic Fracturing through DAS

DAS has recently been used as a means to monitor the hydraulic fracturing process. This monitoring has allowed engineers to detect where they are inducing fractures in real time which enables them to make quick decisions about their operation. When fluid is injected into the formation through perforation clusters, the fluid injection generates a sound that is detected with the sensing fiber along the wellbore. An example of acoustic data taken during a hydraulic fracture operation by Shell is presented in **Fig. 8**.

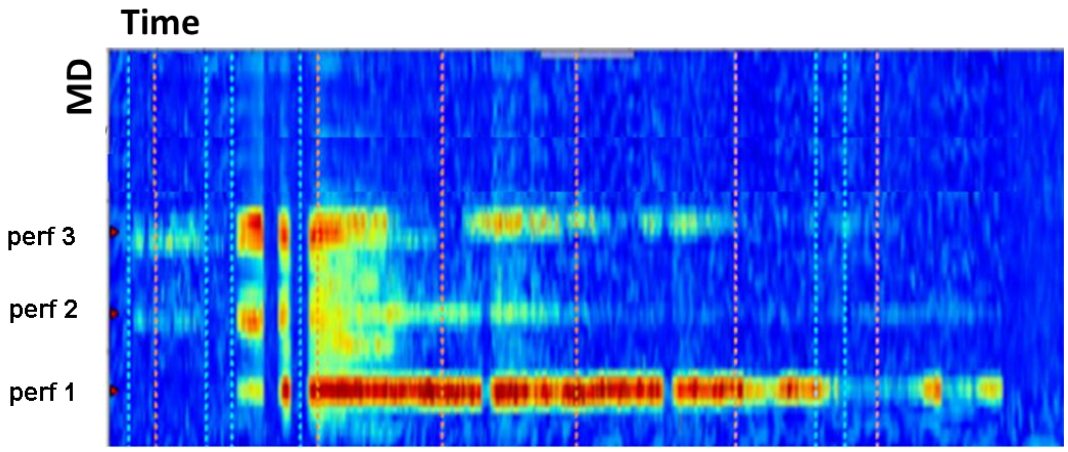

Fig. 8 Monitoring of Hydraulic Fracturing with DAS (Molenaar 2012)

By recording the sound along the length of the wellbore, engineers can determine where fluid is being injected. As seen along the depth of the wellbore over time, sound is generated along three perforation clusters. The dark red signifies a higher sound intensity

while the blue signifies a lower sound intensity. By identifying the sound events through the sound intensity, engineers can determine which cluster is taking the most fluid with the idea that a higher volume of fluid flowing through a perforation generates the greatest sound. From the acoustic data one can deduce that perforation cluster number one took the greatest amount of fluid as the loudest sound is generated in this area for the longest period of time, when compared to the sound recorded at clusters number two and three.

Leak Detection with DAS

With recorded sound along the depth of a well, engineers can determine if and where leaks are occurring. An example of a leak detected through DAS data is presented by OptaSense in **Fig. 9**.

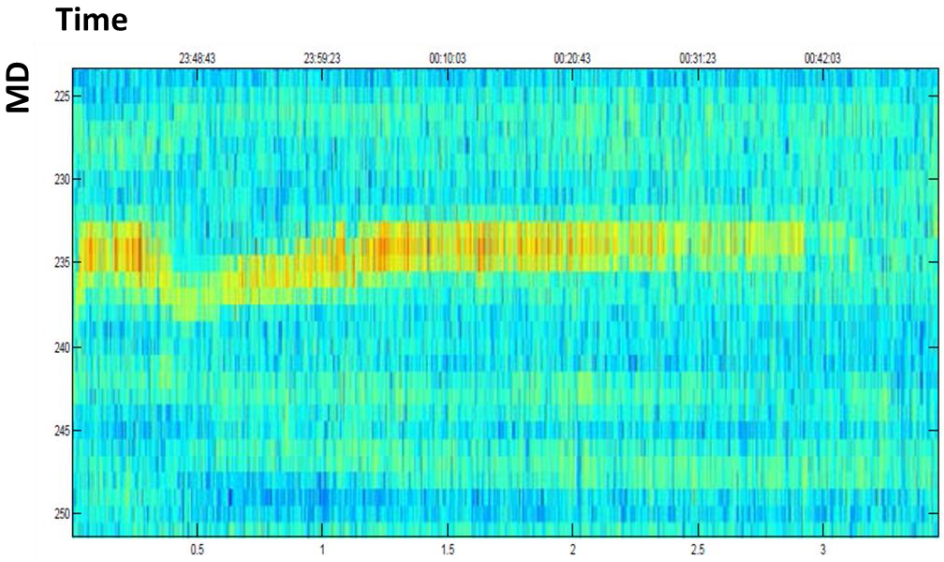

Fig. 9 Fluid Leak Detected Along Wellbore with DAS (Boone et al. 2014)

As seen in **Fig. 9**, an acoustic event occurs at a depth of 236 meters over one hour. Fluid is believed to be leaking through a channel behind the casing as stated by the authors.

Production Monitoring with DAS

Acoustic data during production monitoring can give engineers an indication of where fluid is being produced and the phase of the fluid. Experiments conducted by McKinley et al. (1973) gave an indication that gases produce sound above 1000 Hz and liquids produce sound near 400 Hz when throttled across an orifice. With this simple knowledge, one can determine valuable information about a producing well. An example of DAS data acquired in a producing well is seen in **Fig. 10**.

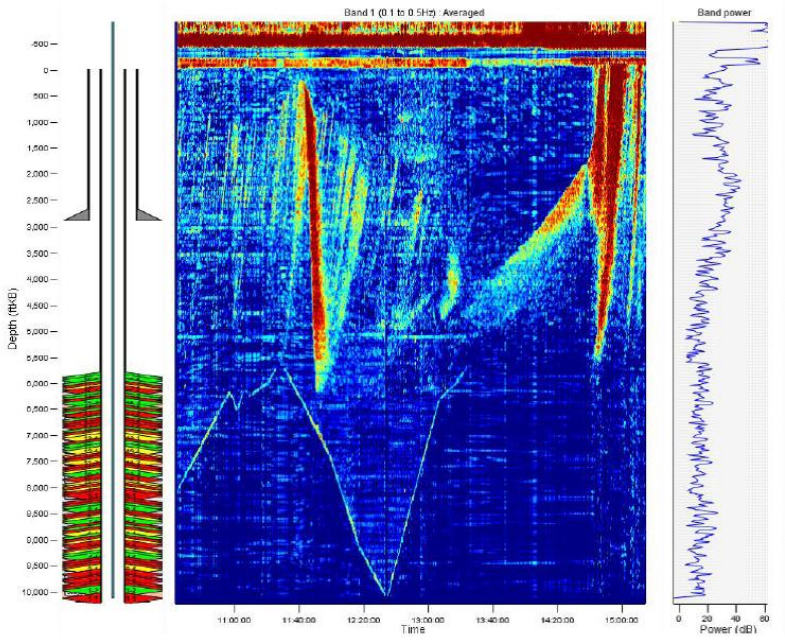

Fig. 10 DAS Data Acquired in a Producing Well (Van der Horst et al. 2014)

Through DAS data acquired in this producing well, the authors were able to determine the zones that produced (displayed in green) and those that did not (displayed in red). By looking at the sound data and how the sound is inconsistently appearing over time in the top half of the well, the authors determined that this well was slugging.

1.2.4 Noise Generation in Wellbores

When fluid is produced, fluid first enters the fracture from the formation and the fluid flows through the proppant filled fracture and finally flows through the perforation tunnel through the cement and casing as depicted in **Fig. 11**.

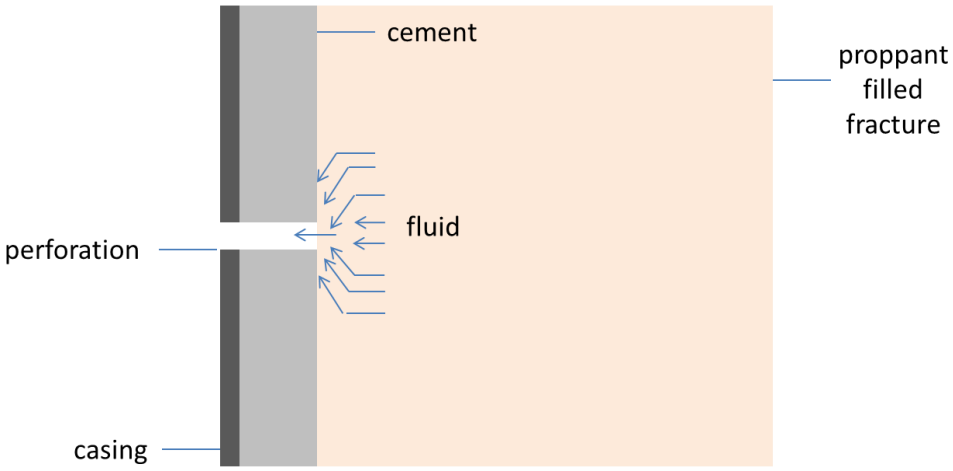

Fig. 11 Flow Path of Fluid Produced (Martinez et al. 2014)

At the tip of the perforation tunnel there is a large transfer of energy to kinetic energy, generating a large velocity inside the perforation tunnel that leads to turbulent

flow. It is believed that this turbulent flow can generate sound as fluid flows from the fracture into the well.

According to Testud et al. (2009) it is widely known that industry pipe systems, valves, taps and orifices whistle when fluid flows through them. Lacombe et al. (2013) explained that this whistling phenomenon is related to the instability of the shear flow. The instability occurs when vortices reach a location where the velocity exhibits a gradient, or in the case of production through a perforation, an abrupt expansion of the fluid downstream of the shear layer (Lacombe et al. 2013). During this process there is a transfer of energy from the fluid moving to vortices that create sound.

Poldervaart et al. (1974) illustrated how vortices can act as an acoustic source in **Fig. 12**. Depicted are vortices created by a jet of fluid exiting a nozzle. The image taken by Poldervaart et al is a representation of what happens when fluid is produced into a well through a perforation. The fluid jet exits the perforation into the well and produces vortices which in turn produce a sound.

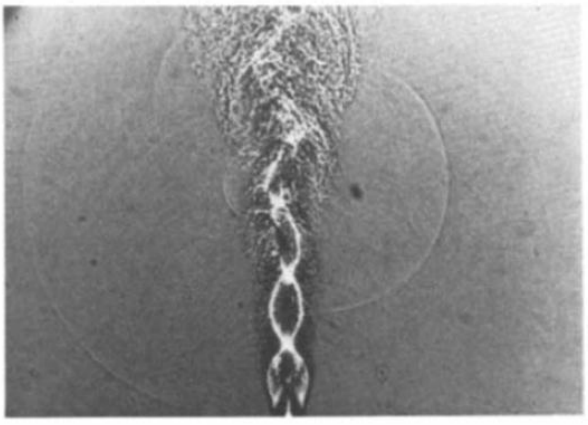

Fig. 12 Visualization of Flow Through a Nozzle (Poldervaart 1974)

Testud et al. (2007) experimental results showed that sound generated from water flowing through an orifice creates a whistling sound which is evident in the dominant peak denoted by f_o in **Fig. 13**.

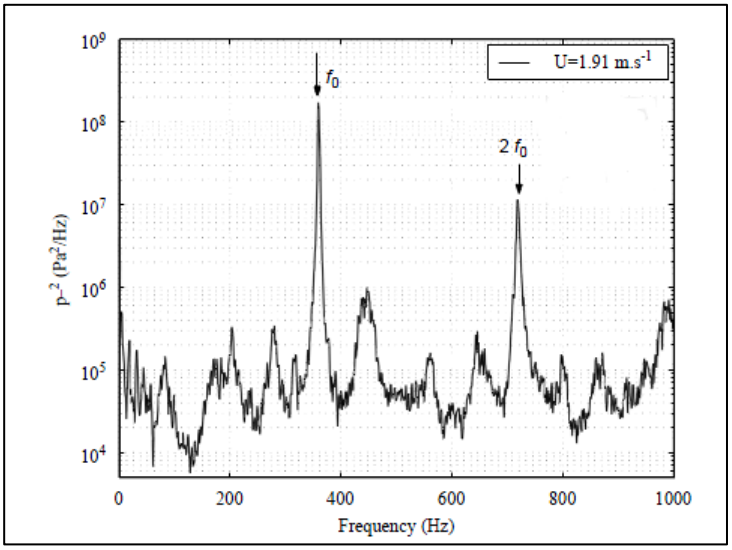

Fig. 13 Sound Spectrum of Fluid Throttled Across Orifice (Testud 2007)

This dominant peak, caused by the whistling phenomenon, is also observed through McKinley's experiment. In the noise spectra presented by McKinley, there is a dominant frequency regardless of flow rate. This is seen in the noise spectra presented in **Fig. 1** and **Fig. 13**.

Two types of flow can be observed when fluid flows through the perforation tunnel into the well, laminar or turbulent flow. In laminar flow, fluid flows in streamlines and fluid layers never mix. In turbulent flow, flow is chaotic and fluid moves in random directions.

Whether a flow is laminar or turbulent is dependent on the flow inertia and fluid friction. The Reynolds number is the ratio of inertial forces to viscous forces. With the characteristic velocity, density, diameter and viscosity, the Reynolds number is expressed as

$$N_{Re} = \frac{\rho v D}{\mu} \quad \text{..... (1.11)}$$

Laminar flow is observed at Reynolds numbers less than 2100 and turbulent flow is observed at Reynolds numbers above 4000. Reynolds numbers between 2100 and 4000 can exhibit both types of flow (Denn, 1980).

At reservoir conditions, the Reynolds number for flow in a perforation tunnel is above the laminar region. The Reynolds number for gas flow through a perforation is estimated to be 3423 in a Barnett shale well producing 10 MMscf/day from a reservoir with a pressure of 4000 psia and temperature of 205°F. The Reynolds number for gas flow through a perforation is estimated to be 2634 in an Eagle Ford well producing 10 MMscf/day from a reservoir with a pressure of 6985 psia and temperature of 270°F. These Reynolds number above 2100 indicate that vortices are likely present in the gas flow through producing perforations. The fluid properties and fluid velocity through a perforation used to calculate the Reynolds numbers are estimated with correlations presented in Appendix A.

1.2.5 Acoustic Waves and Signal Processing

Sound is a pressure wave that is induced by molecular vibrations. When a fluid is set into vibration, the vibrations begin to propagate away from their source. This

propagation of vibrations can be thought of as a transfer of momentum from one molecule to another (Broch 1971).

Sound is characterized by its frequency in Hertz (Hz) and sound pressure level in decibels (dB). A sound's frequency describes the number of cycles of a repetitive wave per second and its sound pressure level is the ratio of the sound pressure to a reference acoustic pressure. In air this reference pressure 20×10^{-6} Pa.

In order to determine the frequency and sound pressure level of sound, an analog signal must first be sampled over time to determine how its amplitude varies over time. Signals are commonly classified as either continuous-time signals or discrete-time signals. Continuous signals are defined at every value in time between a continuous time interval while a discrete signal is defined only at specific time intervals and are usually equally spaced out between time intervals. A discrete time signal is denoted with x(n) while a continuous signal is denoted with x(t), where n is the index of the time instants and t is time.

To sample a continuous-time signal or analog signal, a sampling rate must be decided. In this study we limit ourselves to periodic sampling. The relationship between a discrete and analog signal is denoted by

$$x(n) = x_a(nT), \quad -\infty < n < \infty \quad \text{..... (1.1)}$$

where the discrete-time signal, $x(n)$, is created by sampling the analog signal, $x_a(nT)$, every T seconds. The interval T is the sampling period and is related to the sampling rate by

$$F_s = \frac{1}{T} \quad \text{..... (1.2)}$$

where F_s is the sampling rate in samples per second or the sampling frequency in Hz. According to the Nyquist rate, the lower bound for the sampling rate in Hz is related to f_{max}, the maximum expected frequency.

$$F_s > 2f_{max} \quad \text{..... (1.3)}$$

A sampling rate below twice the maximum expected frequency will cause aliasing.

When an analog signal is sampled above the Nyquist rate, then an alias free signal can be resolved over time. An example of a signal's amplitude plotted over time is shown in **Fig. 14** below.

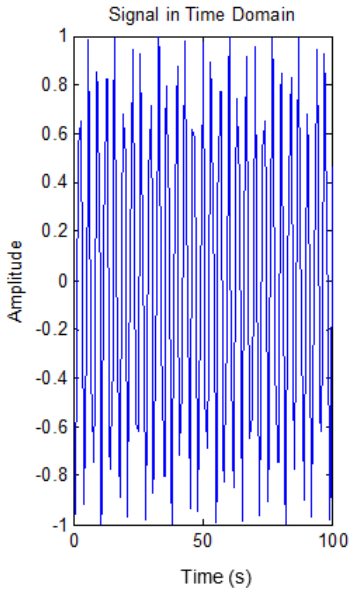

Fig. 14 Sampled Signal in the Time Domain

A signal in the time domain such as the one presented in Fig. 14 can then be transformed into the frequency domain by the Fourier transform. The Fourier transform transforms a signal $x(t)$ into the complex function $X(\omega)$ as follows:

$$X(\omega) = \frac{1}{2\pi}\int_{-\infty}^{\infty} f(t)e^{-j\omega t}\,dt \quad \text{..... (1.4)}$$

The discrete equivalent for a sound signal with N samples is found through:

$$X(k) = \sum_{n=0}^{N-1} x(n)\, e^{-j\frac{2\pi nk}{N}} \quad \text{..... (1.5)}$$

Fig. 15 is an example of the Fast Fourier transform applied to a discrete sound signal in the time domain presented in **Fig. 14**. The frequency peak depicted in **Fig. 15** shows that sound has a mean frequency of 150 cycles per second (Hz).

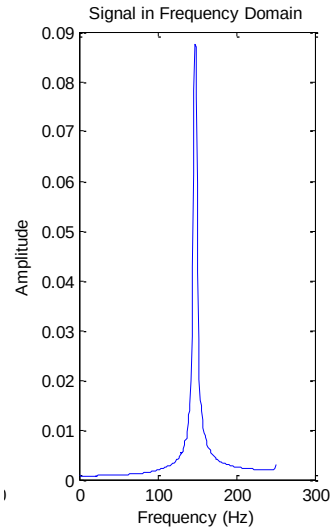

Fig. 15 Time Signal Transformed into the Frequency Domain

In order to transform the time signal into the frequency domain over a specified range of frequencies, a digital filter must be applied. For example, if gas production is

expected to generate noise with a frequency between 1000 and 3000 Hz, but there is loud background noise at 300 Hz, a digital filter can be implemented to the sound recorded so that the sound below 400 Hz does not appear in the frequency spectrum. Implementing a filter becomes important when the sound of interest is not as loud as the background noise. By implementing a filter, one can focus on the sound of interest.

There are three types of filters that are relevant to the signal processing necessary for this study, low pass filters, high pass filters and bandpass filters. An ideal high pass filter passes signals with frequencies above ω_{c1}, while a low pass filter passes signals with frequencies below ω_{c2}. A bandpass filter acts like a low pass and high pass filter in that it will pass signals with frequencies between ω_{c1} and ω_{c2}.

1.3 Problem Description

As seen in the data presented from current operations, DAS data can be used to detect fluid movement. In hydraulic fracturing, DAS data is used to determine where fluid is being injected into the formation; during wellbore monitoring, leaks are detected and their locations identified; and during production monitoring, producing and non-producing zones are identified.

All of the field data presented above have one thing in common, DAS data is used to detect events but not quantify them. The difficulty lies in understanding sound generation and understanding how this sound generation is affected by the flow parameters, such as the fluid properties, velocity and pressure gradient of the fluid.

Understanding how fluid velocity, pressure gradient and fluid properties influence the sound generated would enable engineers to quantify these crucial events. Once understood, engineers could estimate fluid distribution in production and injection across perforations from acoustic data gathered with DAS. It has also been speculated that DAS could be used for sand detection, detecting gas breakthrough, gas lift optimization and ESP monitoring in addition to distributed flow measurements (Johannessen et al. 2012).

1.4 Research Objectives

The main objective of this work is to understand how acoustic data can be used to quantify the events that are being detected. This will render acoustic data to be used as a quantitative tool and not solely for qualitative purposes.

Specific research objectives are outlined as follow:

1. Build an experimental apparatus that can be used to simulate production from a hydraulically fractured well.
2. Record and process sound that is generated when fluid is produced into the simulated well.
3. Determine the relationship between sounds produced and the associated flow rate through experimental results.
4. Propose a method applicable to the field to analyze sound from production to predict flow rates.
5. Quantify the energy from flow that is converted into sound energy.

6. Identify which parameters do not affect the sound being generated during production.

By accomplishing the objectives, this work will enable those interested in DAS to understand how sound is generated and how the sound generated relates to flow rates.

2. LABORATORY APPARATUS AND EXPERIMENTAL PROCEDURE

2.1 Description of Laboratory Apparatus

An experimental apparatus was built to simulate a well with a fracture. The apparatus consists of a large pipe as casing, and a small pipe filled with proppant connected to the large pipe to simulate a fracture behind the perforation. **Fig. 16** below is a picture of the experimental apparatus.

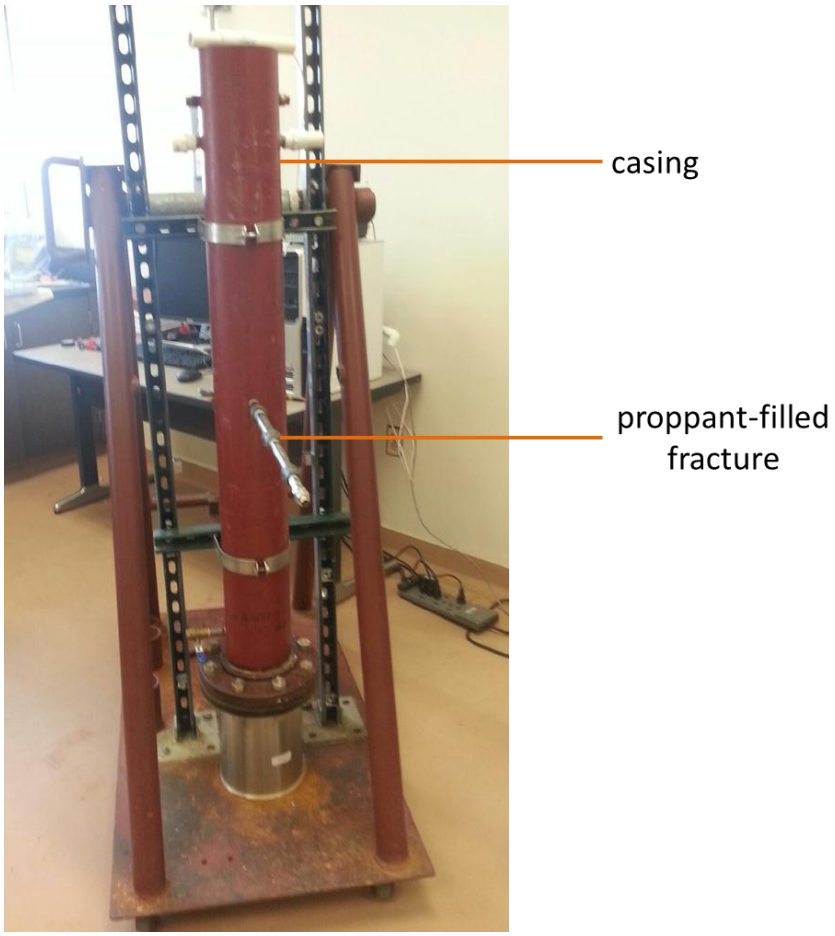

Fig. 16 Experimental Apparatus

The casing pipe is a 3.9 foot long pipe with an inner diameter of 4 7/8 inch. It is propped vertically with a stand. A perforation was created at two feet below the top of the casing. The perforation was threaded for 3/8 inch NPT and the fracture pipe was screwed into the perforation. A single Bruel and Kjaer 8103 type hydrophone was suspended in the casing next to the perforation. This set-up is depicted in **Fig. 17** below.

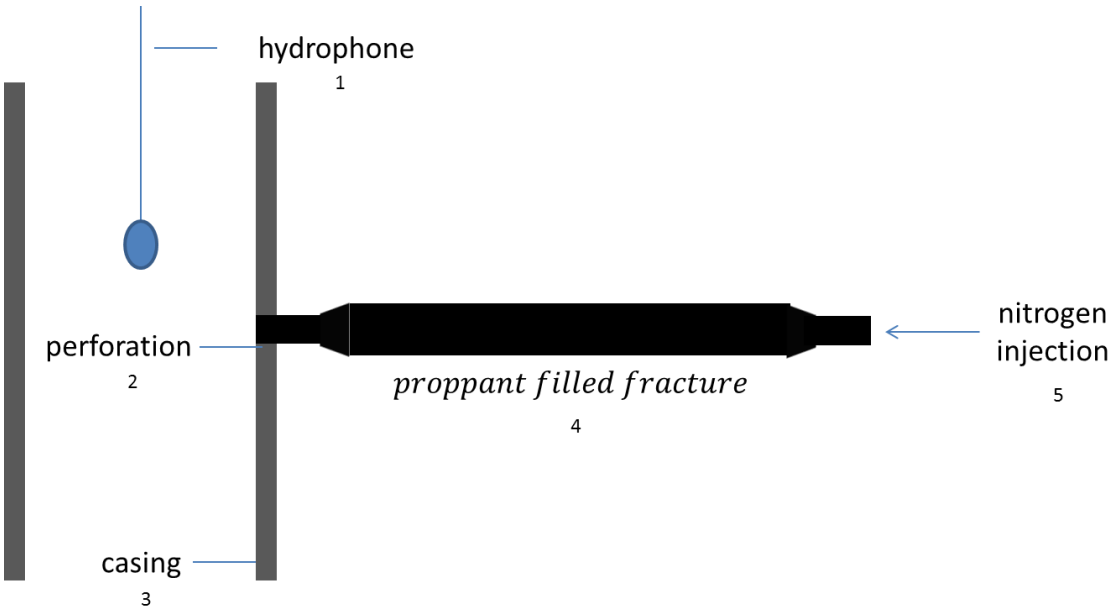

Fig. 17 Experimental Setup (Martinez et al. 2014)

Information for parts labeled one through five can be found in **Table 1**.

Table 1 – Description of Experimental Setup

Number	Item	Specification	Dimensions
1	hydrophone	B&K 8103	cylindrical: 9.5-mm diameter, 25-mm length
2	perforation	stainless steel pipe	3/8-in inner diameter, 2.5-inch length, placed 2 feet down from top of casing
3	casing	stainless steel pipe	4 7/8- in inner diameter, 5.5-in outer diameter, 3.9-ft length
4	proppant filled fracture	stainless steel pipe	diameters used: 3/8, 1/2, 2 in lengths used: 15, 31.7, 48.4 cm

2.2 Signal Processing Components

2.2.1 Hydrophone

A hydrophone is used to collect sound data from experiments. The hydrophone is a Bruel & Kjaer type 8103 hydrophone. The B&K hydrophone can measure in the frequency range of 0.1 Hz to 180 kHz, is omnidirectional and is small enough (50 x 9.5 mm) to fit inside the wellbore. A picture of the hydrophone is found in Fig. 18.

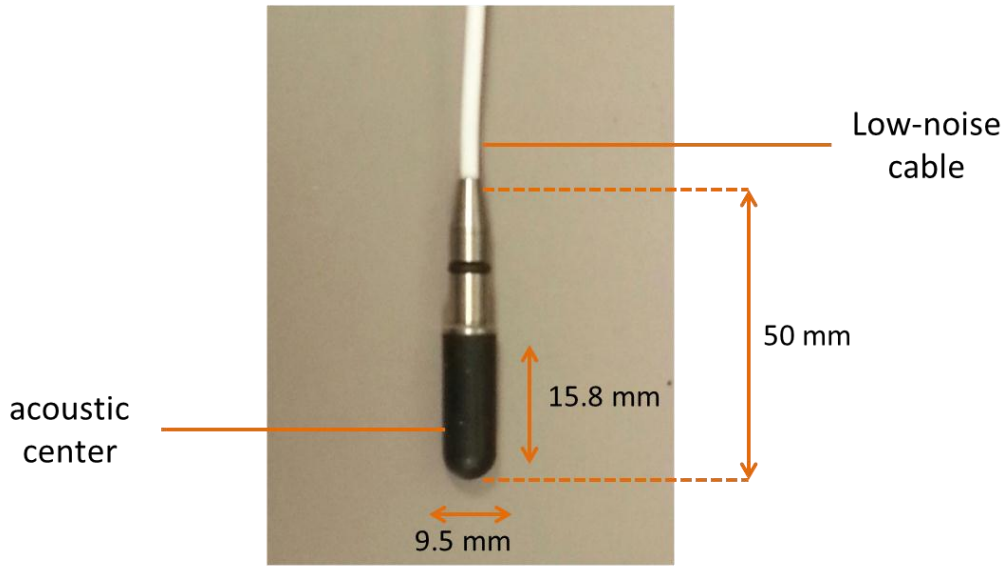

Fig. 18 B&K Hydrophone Type 8103

Hydrophones have a piezoelectric transducer that in the presence of mechanical stress generate a voltage. The voltage is directly related to the pressure of the acoustic wave by the out unit amplification specified by the charge amplifier. Hydrophones transform pressure waves into electrical signals with units of Volts/time. In order to transform the wave back to the correct units in Pa, each point must be divided by the constant specified by the charge amplifier during the experiment which has units of volts/Pa.

2.2.2 Charge Amplifier

A charge amplifier is necessary to condition the signals collected by the hydrophone. The charge amplifier powers the hydrophone and amplifies the signal

recorded which enables the signal to reach the data acquisition device. A picture of the charge amplifier is found in **Fig. 19**.

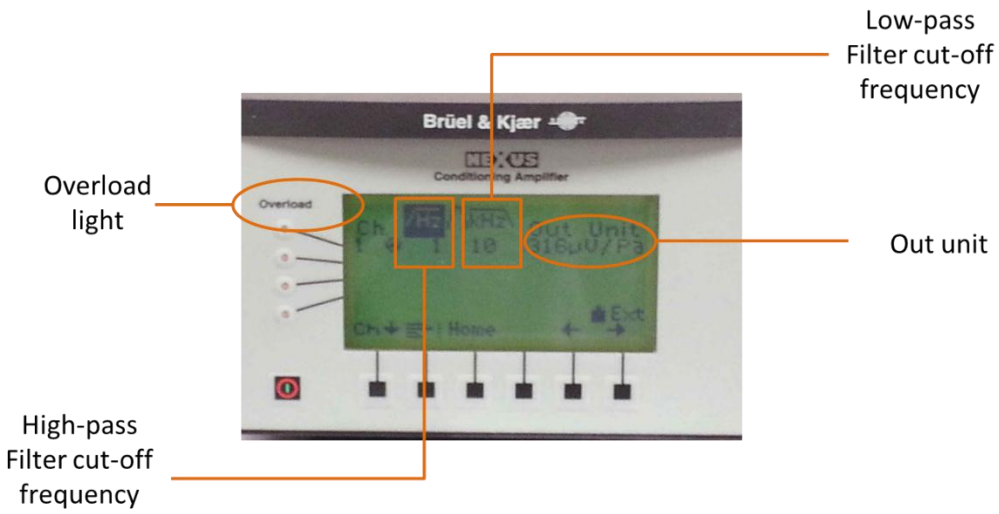

Fig. 19 Bruel & Kjaer Nexus Conditioning Signal Amplifier

The charge amplifier has several settings that must be configured for each experiment. On the control panel of the amplifier shown above, there are three parameters that must be set for each experiment, including the frequency range of the bandpass filter and the output unit. The conditioning amplifier implements a bandpass filter to the signal collected. The bandpass filter range was set from 1 Hz to 10 kHz for the experiments. The output unit changed depending on the strength of the sound signal. The limitation to the out unit is the voltage range that the data acquisition device can read. The NI 9234 can process a signal with magnitude of five volts. If a signal with a

voltage magnitude greater than five is generated, the overload indicator lights up in red signifying that the out unit should be decreased.

2.2.3 Data Acquisition Device

The NI 9234 is a data acquisition module that is designed for multiple channel count sound and vibration applications. In the experiments conducted, only one hydrophone was used and so one channel was used out of the four available. The device implements a sample rate of 51.2 kS/s and has a limited voltage range of -5 V to +5 V. In order to collect data, the magnitude of the signal collected must be within the specified range mentioned. The output voltage from the hydrophone can be decreased or increased with the charge amplifier as explained in the previous section. A picture of the DAQ device is found in **Fig. 20**.

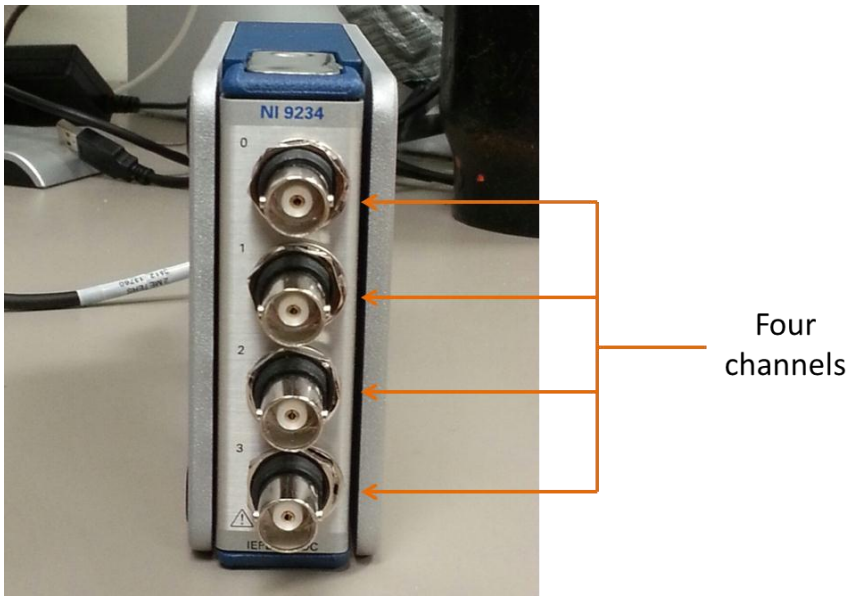

Fig. 20 National Instrument 9234 Data Acquisition Device

2.2.4 Signal Processing Software

LabVIEW is used to collect signals that are acquired with the DAQ device. A schematic of the workflow created in LabVIEW is presented in **Fig. 21**.

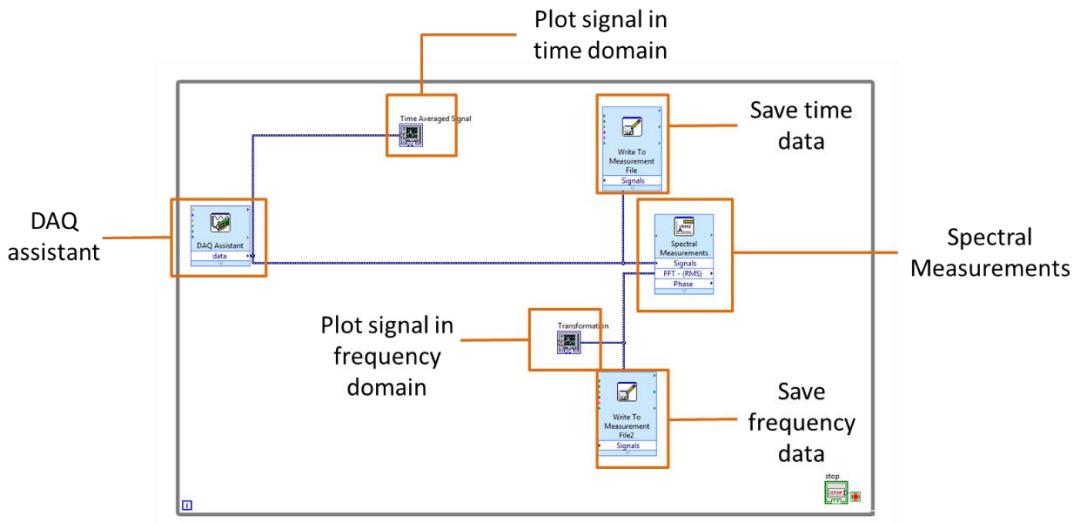

Fig. 21 LabVIEW Worksheet

The workflow consist of a DAQ assistant, graphing blocks, spectral measurements and blocks which write the data to excel sheets. The DAQ assistant is used to specify the settings of the NI 9234 DAQ device.

The plotting blocks plot the signal in the time and frequency domain after N samples are sampled as shown in **Fig. 22**.

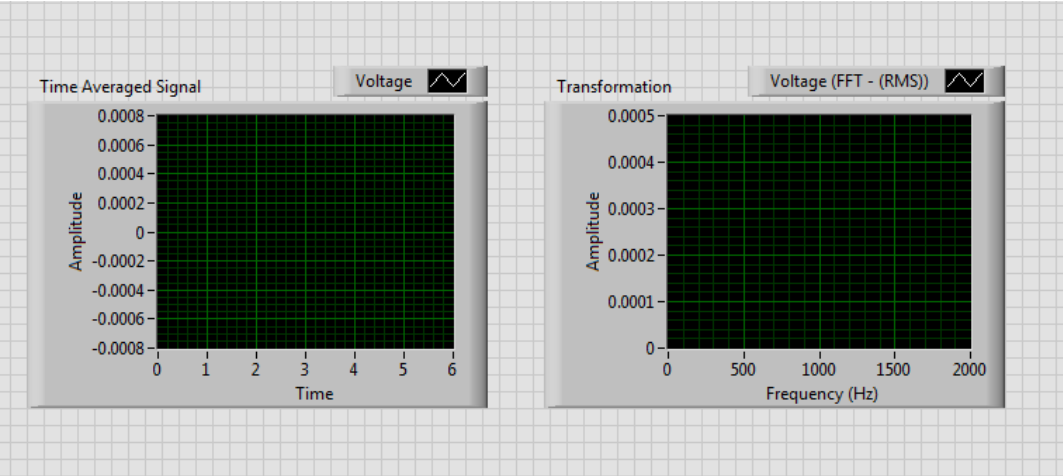

Fig. 22 Plots Generated in LabVIEW

The plots generated in LabVIEW are not used for analysis but instead to monitor the data that is being recorded during the experiments. The data that is recorded are saved into Excel sheets.

Sound signal data are uploaded from the saved Excel sheets into MATLAB where signal processing is implemented. The built in functions, Butterworth bandpass filter and the Fast Fourier Transform, are implemented to first process the signal and then plot the frequency spectrum.

2.3 Experimental Procedures

2.3.1 Preparing Signal Processing Components

The signal processing components must be set up adequately in order to have successful data collection. **Fig. 23** shows how the signal processing components must be arranged.

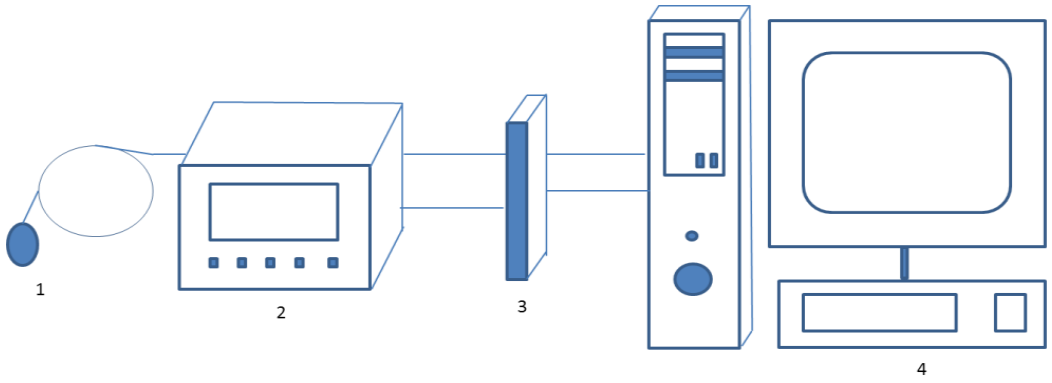

Fig. 23 Signal Processing Components (Martinez et al. 2014)

The hydrophone is connected to the charge amplifier by a Baynoet Neill-Concelman (BNC) connector. A depiction of a BNC connection is shown in **Fig. 24**. The charge amplifier is connected to the DAQ device by a BNC connection. The DAQ device connects and transfers data via a USB Male A to B cable to the computer. A summary of each of the signal processing components is presented in **Table 2**.

Fig. 24 BNC Connection

Table 2 – Description of Signal Processing Components

Number	Item	Description	Specifications
1	Hydrophone	B&K 8103	voltage sensitivity: 26.4 micro volts/Pascal
2	conditioning amplifier	NEXUS Conditioning Amplifier Type 2690	amplification: 0.0316 millivolt/Pascal low-pass filter: 1 Hz high-pass filter: 10 Hz
3	data acquisition device	NI-9234	-5V to +5V range
4	computer software	LabVIEW	LabVIEW was used to collect data sampling frequency: 22 kHz samples read: 220 kHz
4	computer software	MATLAB	Built in functions used to process data: Butterworth band-pass filter FFT (fast Fourier transform)

Configuring the data acquisition device through LabVIEW's DAQ assistant is important to correctly acquire data from the hydrophone. **Fig. 25** shows the DAQ assistant window used when configuring the channel settings.

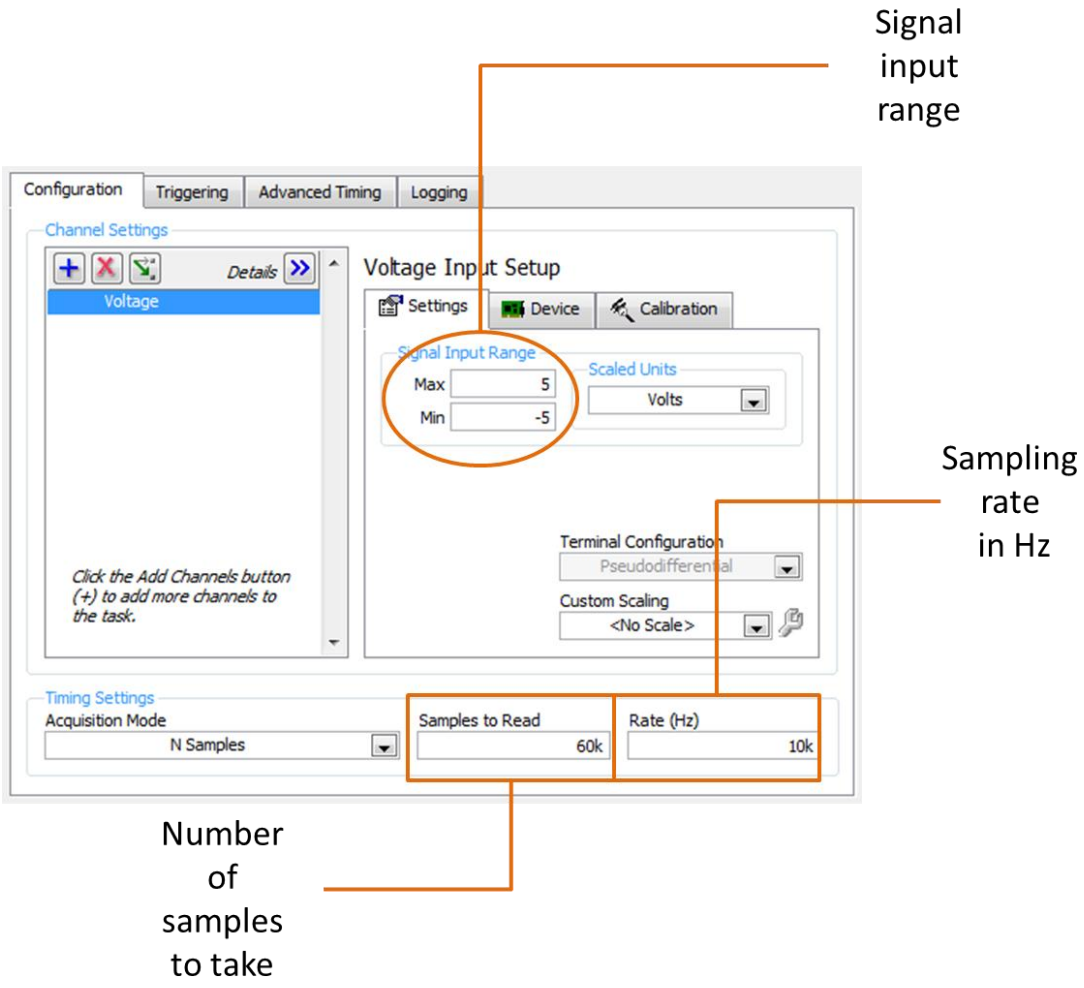

Fig. 25 DAQ Device Settings

The following settings are essential for the proper sound data collection: signal input range and its units and the time settings such as the acquisition mode, samples to

read and the sampling rate. The signal input range is set from -5 to 5 volts as this is the signal limit on the NI 9234 DAQ device. The sampling rate in Hz should be set to twice the expected frequency in Hz as described in the signal processing section. The acquisition mode should be set to N samples and the number of samples to read depend on the desired acquisition time. If the desired acquisition time is 10 seconds and the sampling rate is set to 10 kHz, then the number of samples to read should be calculated as follows:

$$N\ samples = desired\ time(s) \times rate(Hz) \quad \text{..... (2.1)}$$

$$N\ samples = 10\ s \times 10\ kHz = 100{,}000 \quad \text{..... (2.2)}$$

In order to sample for 10 seconds at a sampling rate of 10 kHz, 100,000 samples must be taken.

2.3.2 Preparing Laboratory Apparatus

Fluid is injected into a proppant filled pipe into the well and sound is recorded with a B&K type 8103 hydrophone. Experiments are conducted with different proppants in the proppant filled fracture. The proppants used are ceramic and sands. **Fig. 26** below depicts the three different proppants used.

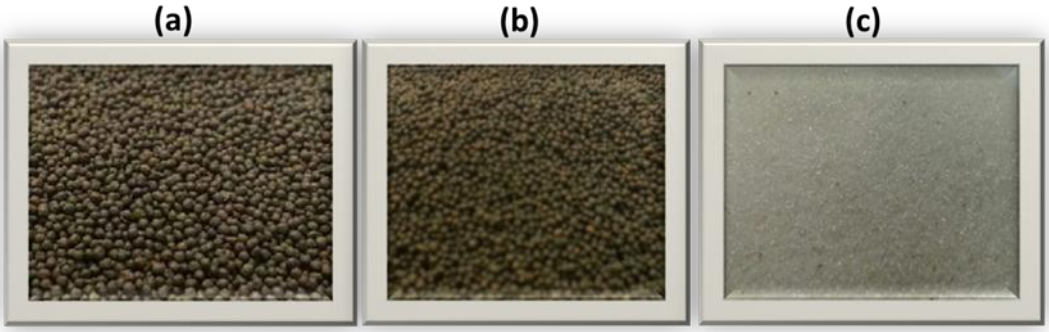

Fig. 26 Proppant Size (A) 20/40 Mesh (B) 16/30 Mesh (C) 30/50 Mesh

The 20/40 mesh and 16/30 mesh proppants are both ceramics and the 30/50 mesh proppant is a sand. The proppant is loaded into the fracture pipe shown in **Fig. 27** below.

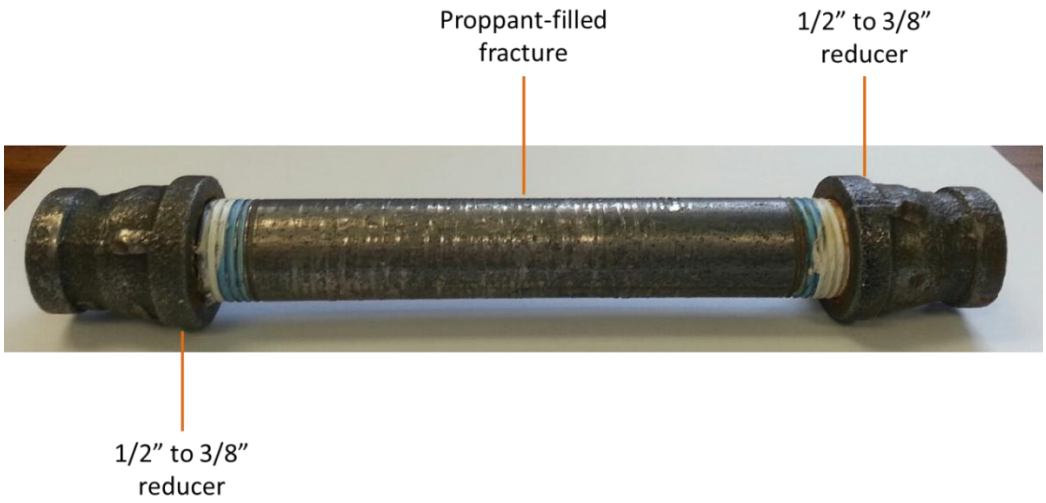

Fig. 27 Proppant Filled Pipe

The proppant in the center pipe is contained with a mesh that is set between the end of the pipe and the pipe couplers. The pipe couplers reduce from 1/2 inch NPT to 3/8 inch NPT. The mesh used can be seen in **Fig. 28**.

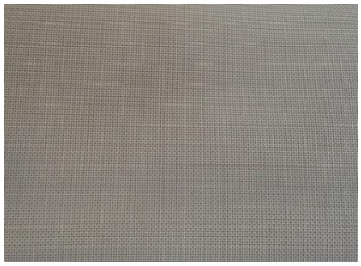

Fig. 28 Mesh Screen

Nitrogen is injected into the end of the fracture pipe, with a 1/4 inch inner diameter tubing and so a reduction from 3/8 inch to 1/4 inch tubing is necessary. This is done with the following set up depicted in **Fig. 29**.

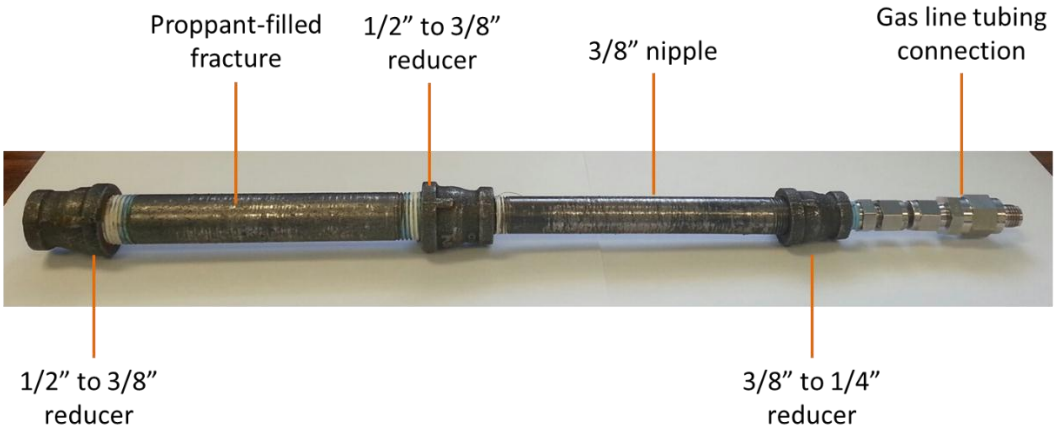

Fig. 29 Connection to Nitrogen tank

A 6 inch long 3/8 inch NPT nipple is connected to the fracture pipe through the reducer on one end and at the other end it is reduced to ¼" NPT.

The injection rate into the proppant filled pipe is controlled with the nitrogen injection pressure. A pressure regulator shown in **Fig. 30** is used to regulate the injection pressure between 10 to 160 psig.

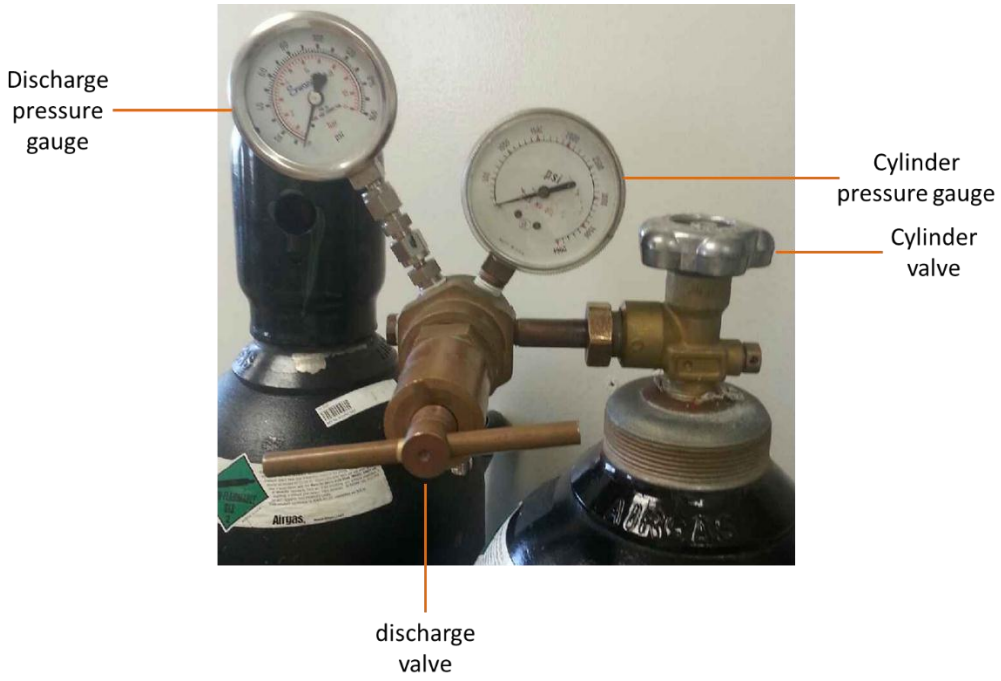

Fig. 30 Pressure Regulator

The pressure regulator is connected to the tank and reads the pressure of the tank when opened with the pressure gauge on the right. The pressure gauge on the left reads the discharge pressure when the valve on the pressure regulator is opened. During

injection, the valve on the cylinder is opened and the valve on the pressure regulator is opened to the desired discharge pressure.

When the fracture is filled with proppant and connected to the perforation then the gas line from the nitrogen cylinder can be connected to the proppant filled pipe. The final experiment setup is shown in **Fig. 31**.

Fig. 31 Fully Assembled Experimental Apparatus

2.3.3 Conducting Sound Measurements

Experiments were conducted on different fracture-pipe lengths, fracture-pipe diameters, proppant sizes and injection pressures. A summary of the experiments conducted are found in **Table 3**. The detailed procedure for conducting an experiment is outlined below:

1. Load the appropriate sized proppant into the fracture pipe. Ensure that one reducer with the mesh is on one end of the pipe.
2. Once loaded, screw on the reducer to the opposite end of the pipe.
3. Screw the perforation tunnel onto the reducer and then screw the perforation tunnel into the perforation in the well.
4. Attach the set of pipes and reducers shown in **Fig. 29** to attach the 1/4 inch line from the nitrogen tank.
5. Ensure that the line from the nitrogen tank is attached properly to the fracture pipe and to the pressure regulator on the nitrogen tank.
6. Ensure that the valve on the pressure regulator is closed and then open the valve on the nitrogen tank. The pressure gauge on the right shown in **Fig. 30** should read the pressure of the tank.
7. Slowly open the valve on the pressure regulator up to the point where the pressure regulator on the left in **Fig. 30** reads 10 psig.
8. Locate leaks or loss of nitrogen at any of the connections. If there are leaks, close the valve on the pressure regulator and retighten the connections. Open the valve on the pressure regulator and ensure that there are no further leaks. If there are persisting leaks, reapply Teflon tape to threads where leak is reoccurring. All leaks must be stopped before conducting experiments.
9. Once all leaks are sealed, turn on the charge amplifier and have LabVIEW collect data and plot in real time. Adjust the charge output to ensure that the

signal does not have a magnitude greater than 5 V. If the signal is within the range, take note of the charge output unit.

10. Close the valve on the pressure regulator and determine the sampling rate and number of samples to read. The sampling rate should be kept constant throughout all experiments, nothing lower than 10 kHz is an acceptable sampling rate for gas experiments. The number of samples should give a sampling time of at least 10 seconds. The number of samples is greatly influenced by the supply of gas. Due to the large permeability in the fracture pipe, the nitrogen cylinder can be emptied within minutes during an experiment. At higher injection rates use a sampling time of 5 seconds for a total of 7 experiments, which is 35 seconds of data.
11. Once the sampling rate and number of samples are entered into the DAQ assistant in LabVIEW, open the pressure regulator to 10 psig and start sampling with LabVIEW. After seven data sets, increase the injection pressure by an increment of 10 psig and restart sampling with LabVIEW. Continue increasing the discharge pressure by increments of 10 psig and restarting the data collection with LabVIEW until reaching a discharge pressure of 160 psig.
12. If the discharge pressure is unstable, discontinue experiments and move on to the next experiments. Reaching an injection pressure of 160 psig may not be possible for some experiments due to the high permeability of the fracture.
13. After conducting experiments with the fracture length of 15 cm, disconnect the perforation tunnel from the perforation and connect to a rotameter. The flow rate

for each injection pressure must be recorded. Open the valve on the pressure regulator and read the flow rate on the rotameter. Repeat this in increments of 10 psig until the final pressure of 160 psig is reached.

14. After the flow rate is measured, increase the fracture length to 31.7 cm, reconnect the perforation tunnel to the perforation and repeat the experiments.

15. After conducting experiments with the fracture length of 31.7 cm, increase the fracture length to 48.4 cm and repeat the experimental procedures outlined.

16. After conducting experiments with 16/30 mesh proppant and fracture lengths of 15, 31.7 and 48.4 cm, repeat experiments with the 20/40 mesh and 30/50 mesh, for each of the fracture lengths of 15, 31.7 and 48.4 cm.

17. After conducting experiments with the different fracture lengths and proppant sizes, repeat the experiments with 16/30 mesh for each of the pipe diameters of 3/8, 1/2 and 2 inches. The fracture lengths for these pipe diameters should be six inches.

18. For each of the time signals saved with LabVIEW on excel sheets, upload into MATLAB and implement a band-pass filter and then implement the FFT to the filtered signal and plot the frequency spectrum. Please refer to the signal processing section.

Table 3 – Summary of Experiments Conducted

Experiment	Proppant Size	Fracture Length (cm)	Injection Pressure (psig)
1	16/30 mesh	15, 31.7, 48.4	10-160, in 10 psig increments
2	20/40 mesh	15, 31.7, 48.4	10-160, in 10 psig increments
3	30/50 mesh	15, 31.7, 48.4	10-160, in 10 psig increments

2.3.4 Processing Sound

Once experiments are finished, the sound collected from the experiments must be processed and analyzed. The procedure for processing the sound is outlined below:

1. Upload the time and amplitude data saved onto excel sheets from the experiments into MATLAB. MATLAB script used can be found in Apendix B.
2. Implement a band-pass filter to the time data, with lower frequency bounds of 400 Hz and an upper frequency bound of 7000 Hz.
3. Using the built in function, implement the FFT to the filter signal and plot the frequency spectrum.
4. Using the built in function, implement the short time Fourier transform (STFT) to the filtered signal and plot the STFT.

5. To determine the overall sound pressure level, square each of the peak pressures from the FFT and sum them, then divide this sum by a reference pressure squared and then take the 10 base log of this number and multiply by 10. The equation is summarized below

$$L_{SP} = 10\log_{10}\left(\frac{\sum P_i^2}{P_{ref}^2}\right), \quad p_i = p_1, p_2, p_3 \quad \text{..... (2.3)}$$

In equation 2.3 above, the reference acoustic pressure is 20×10^{-6} Pa.

3. EXPERIMENTAL RESULTS AND DISCUSSION

3.1 Sound from Production

3.1.1 20/40 Mesh Experiments

The sound spectrum as seen in **Fig. 32** contains a dominant peak similar to one presented by the work of Testud et al. The dominant peak occurs at 1000-1500 Hz, and the frequency range is in agreement with the work reported by McKinley et al. for sound produced from throttling gas through a channel.

By implementing a short-time Fourier transform (STFT) and fast Fourier transform (FFT), we can determine the sound pressure level and frequency of sound in time. These two transforms were implemented on the sound signal measured for the three proppant sizes, at their highest and lowest injection pressure. As the injection pressure decreases the amplitude of the peaks decreases as well. However, the peaks present at the highest and lowest injection pressure were still present.

The transforms for the experiments with the pipe filled with 20/40 mesh ceramic proppant are shown in **Fig. 32** and **Fig. 33**. From **Fig. 33** we can deduce that there is a dominant peak at 1500 Hz which is present throughout all of the experiments regardless of fracture length and injection rate. The amplitude of these peaks in **Fig. 32** decrease in magnitude with a reducing injection rate.

3.1.2 16/30 Mesh Experiments

The transforms for the experiments with the pipe filled with 16/30 mesh ceramic proppant are shown in **Fig. 34** and **Fig. 35**. From **Fig. 35** we can deduce that there is a dominant peak at 1500 Hz and is present throughout all of the experiments regardless of fracture length and injection rate. The amplitude of these peaks in **Fig. 34** decrease in magnitude with a reducing injection rate. The results from the 16/30 mesh show similar results to that from the experiments conducted with the 20/40 mesh.

3.1.3 30/50 Mesh Experiments

The transforms for the experiments with the pipe filled with 30/50 mesh sand proppant are shown in **Fig. 36** and **Fig. 37**. From **Fig. 37** we can deduce that there is a dominant peak at 1500 Hz and is present throughout all of the experiments regardless of fracture length and injection rate. The amplitude of these peaks in **Fig. 36** decrease in magnitude with a reducing injection rate. The results from the 30/50 mesh show similar results to that from the experiments conducted with the 20/40 mesh and 16/30 mesh.

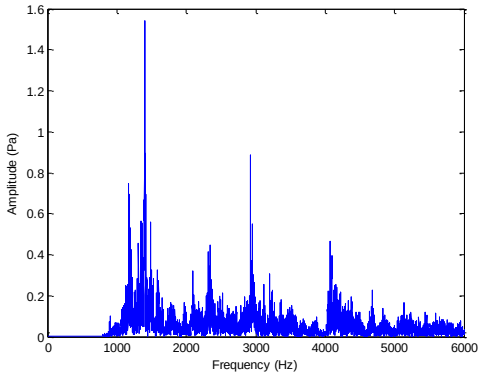

(a) 120 psig injection into length L

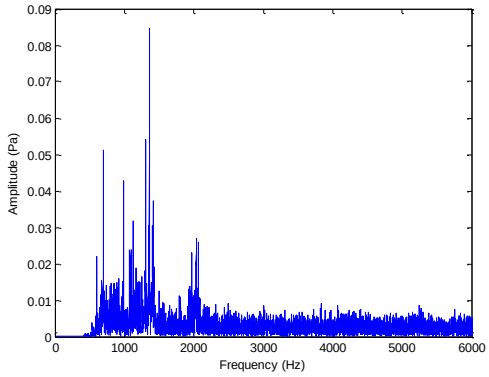

(b) 10 psig injection into length L

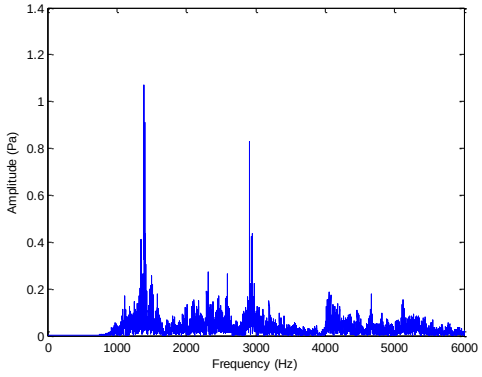

(c) 140 psig injection into length 2L

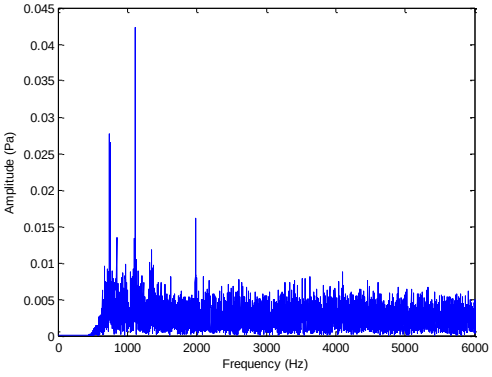

(d) 10 psig injection into length 2L

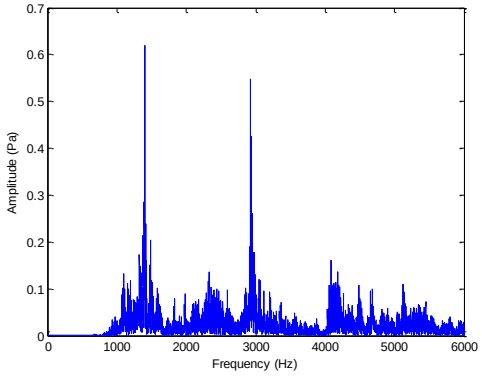

(e) 150 psig injection into length 3L

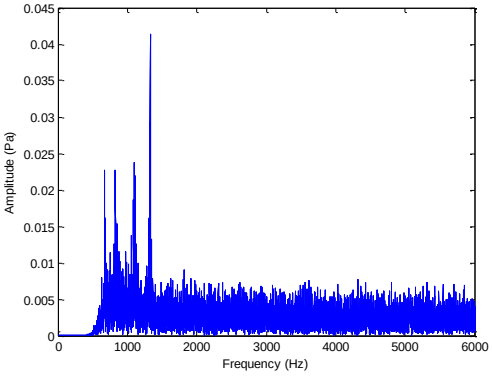

(f) 10 psig injection into length 3L

Fig. 32 Sound Spectrum for Fluid Production from 20/40 Mesh Proppant

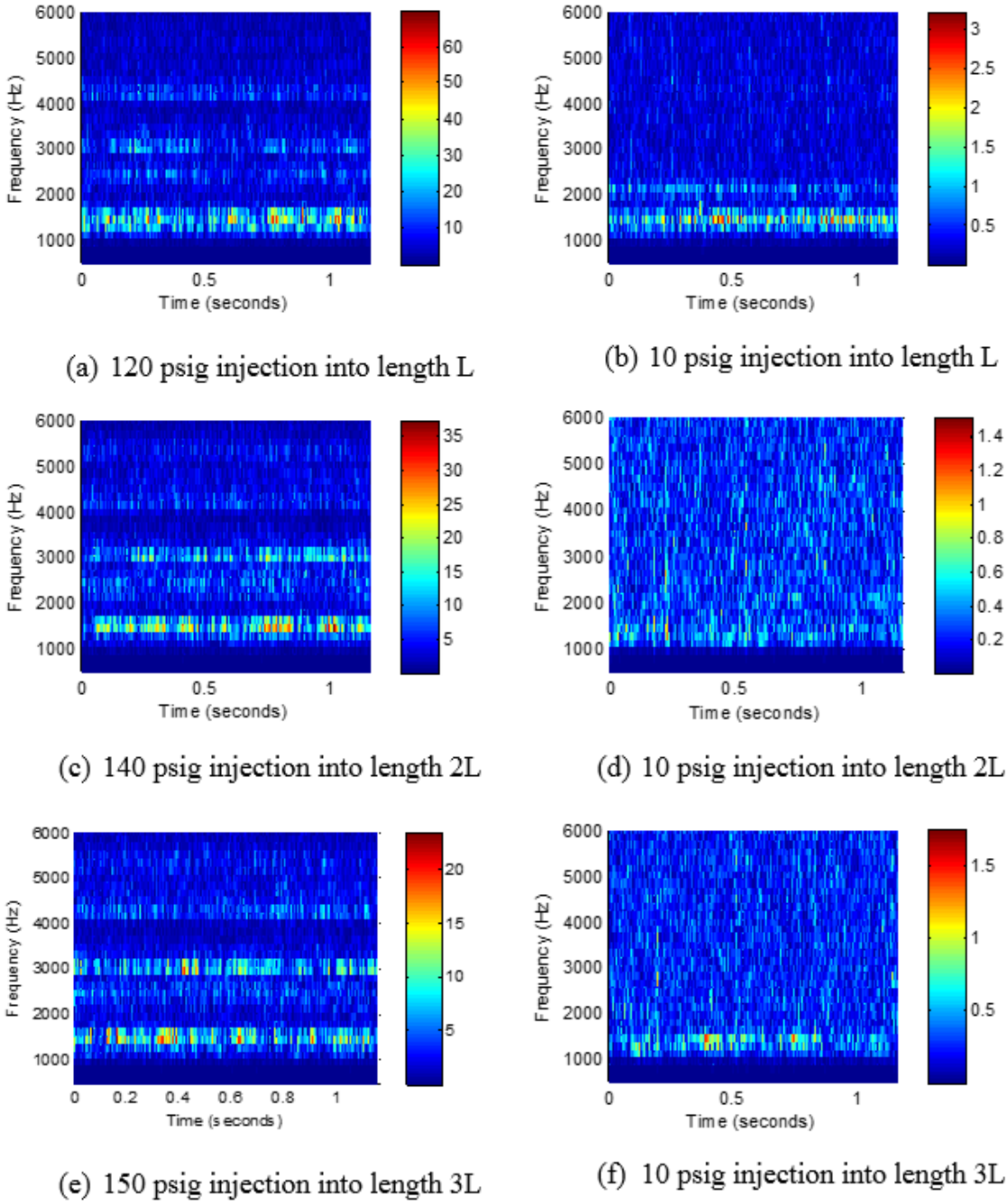

Fig. 33 STFT for Fluid Production from 20/40 Mesh Proppant

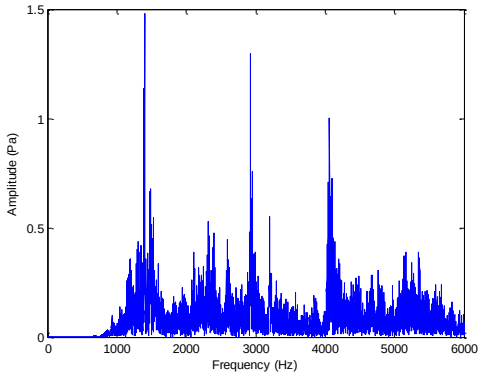

(a) 160 psig injection into length L

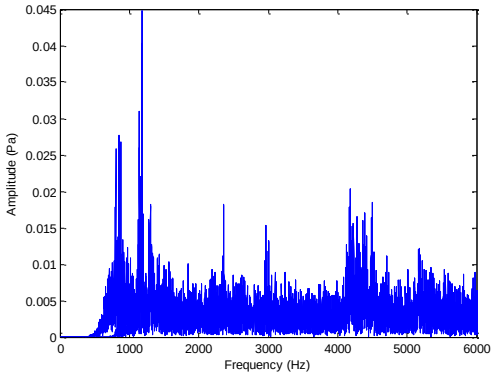

(b) 10 psig injection into length L

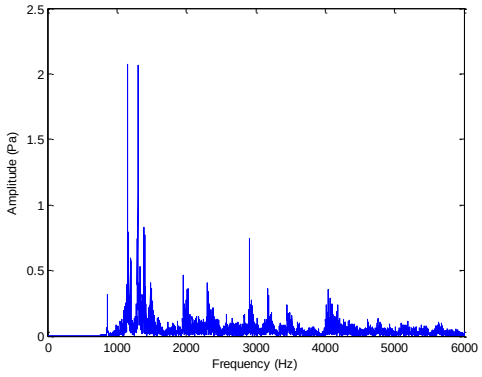

(c) 140 psig injection into length 2L

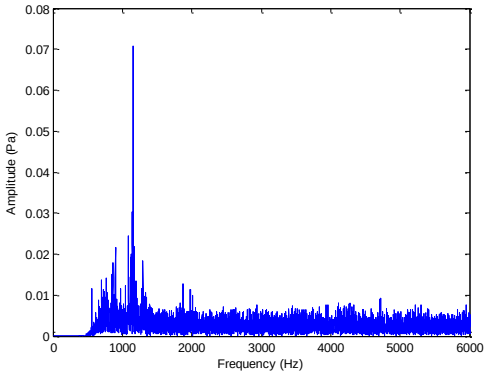

(d) 10 psig injection into length 2L

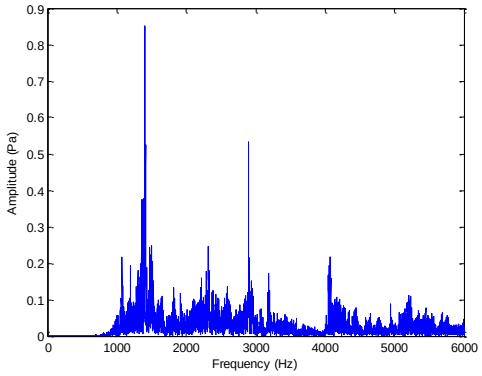

(e) 160 psig injection into length 3L

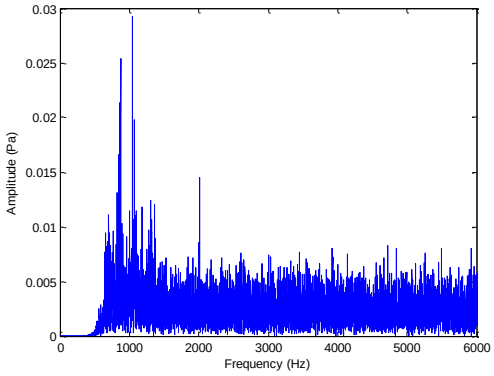

(f) 10 psig injection into length 3L

Fig. 34 Sound Spectrum for Fluid Production from 16/30 Mesh Proppant

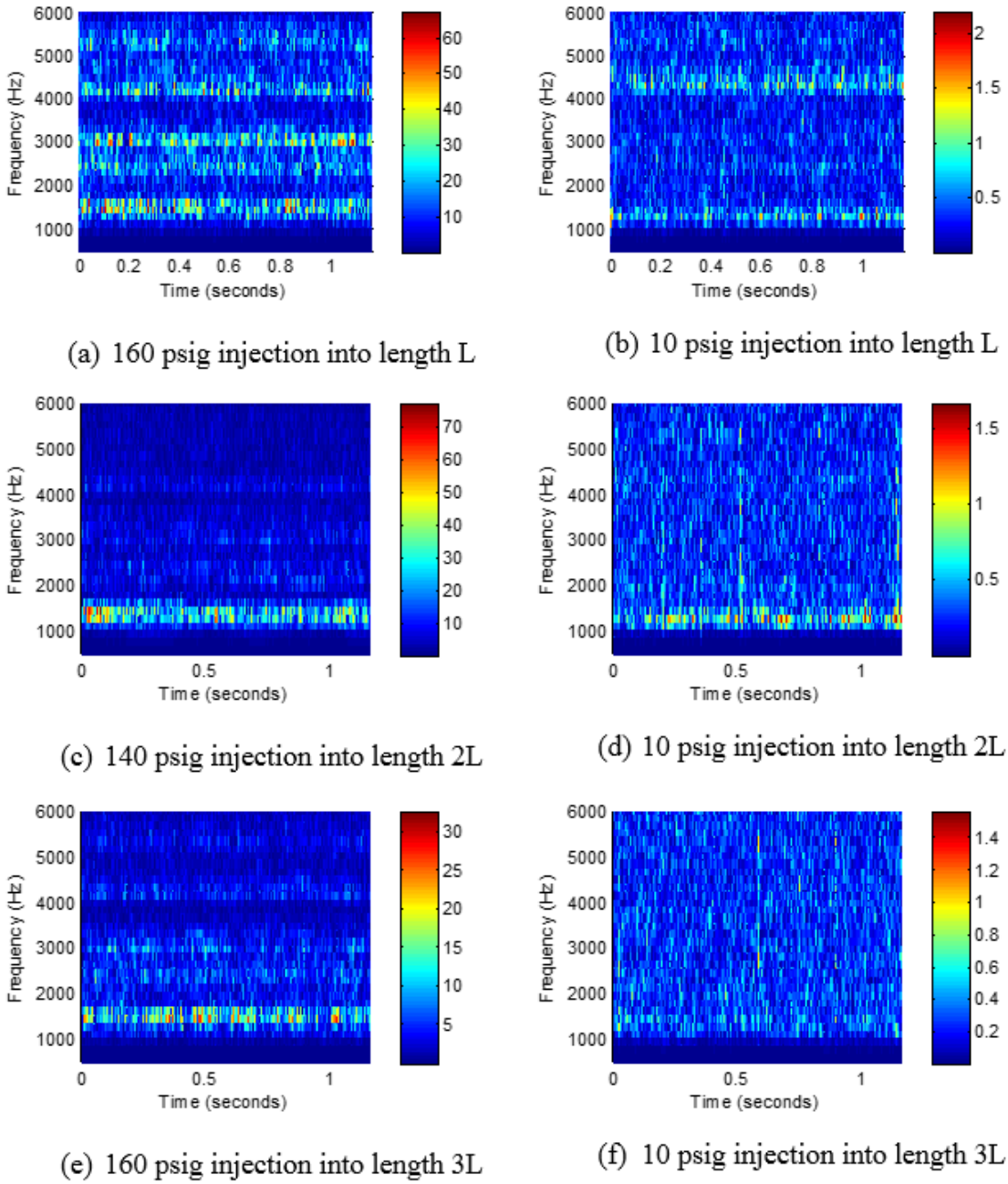

Fig. 35 STFT for Fluid Production from 16/30 Mesh Proppant

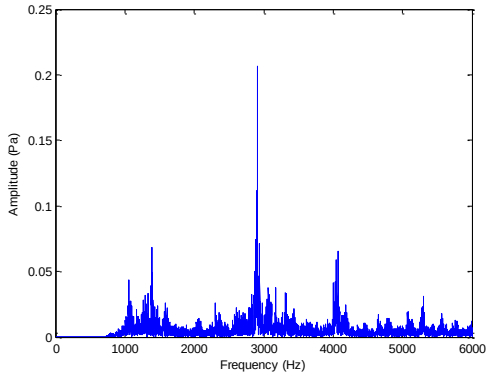

(a) 160 psig injection into length L

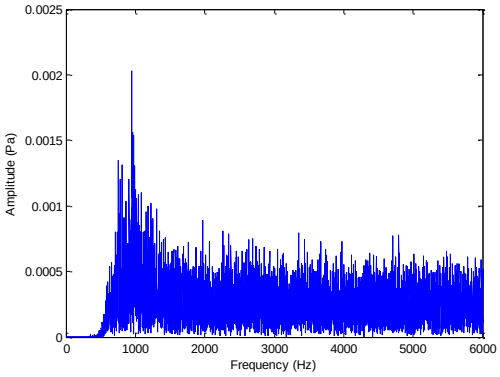

(b) 10 psig injection into length L

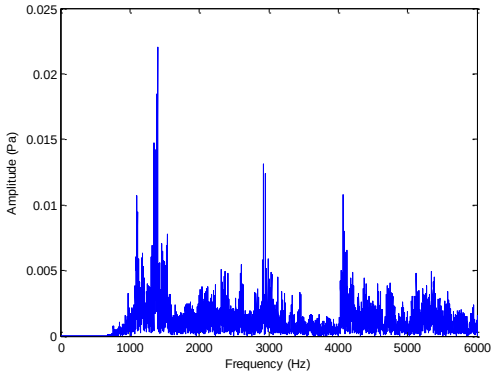

(c) 160 psig injection into length 2L

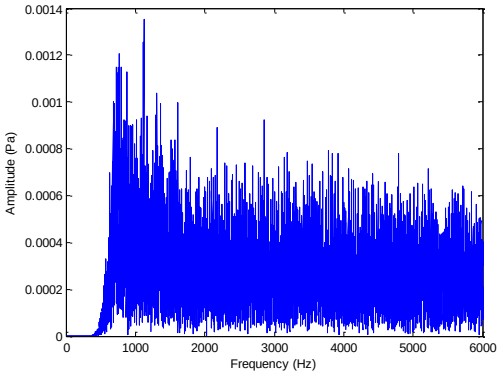

(d) 10 psig injection into length 2L

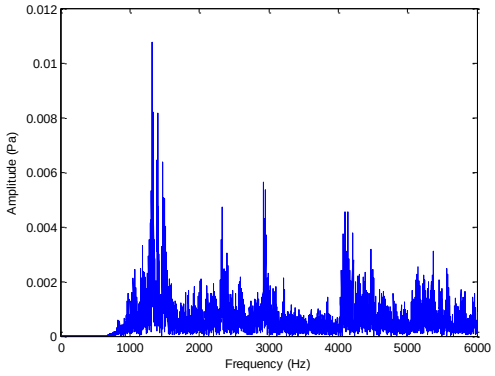

(e) 160 psig injection into length 3L

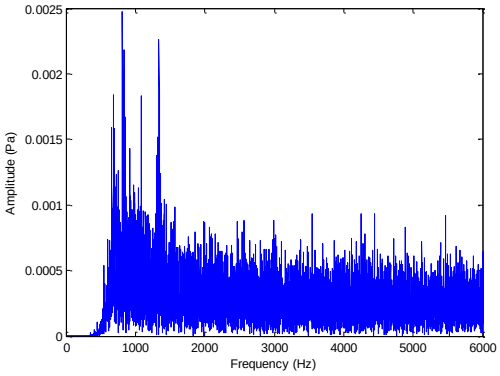

(f) 10 psig injection into length 3L

Fig. 36 Sound Spectrum for Fluid Production from 30/50 Mesh Proppant

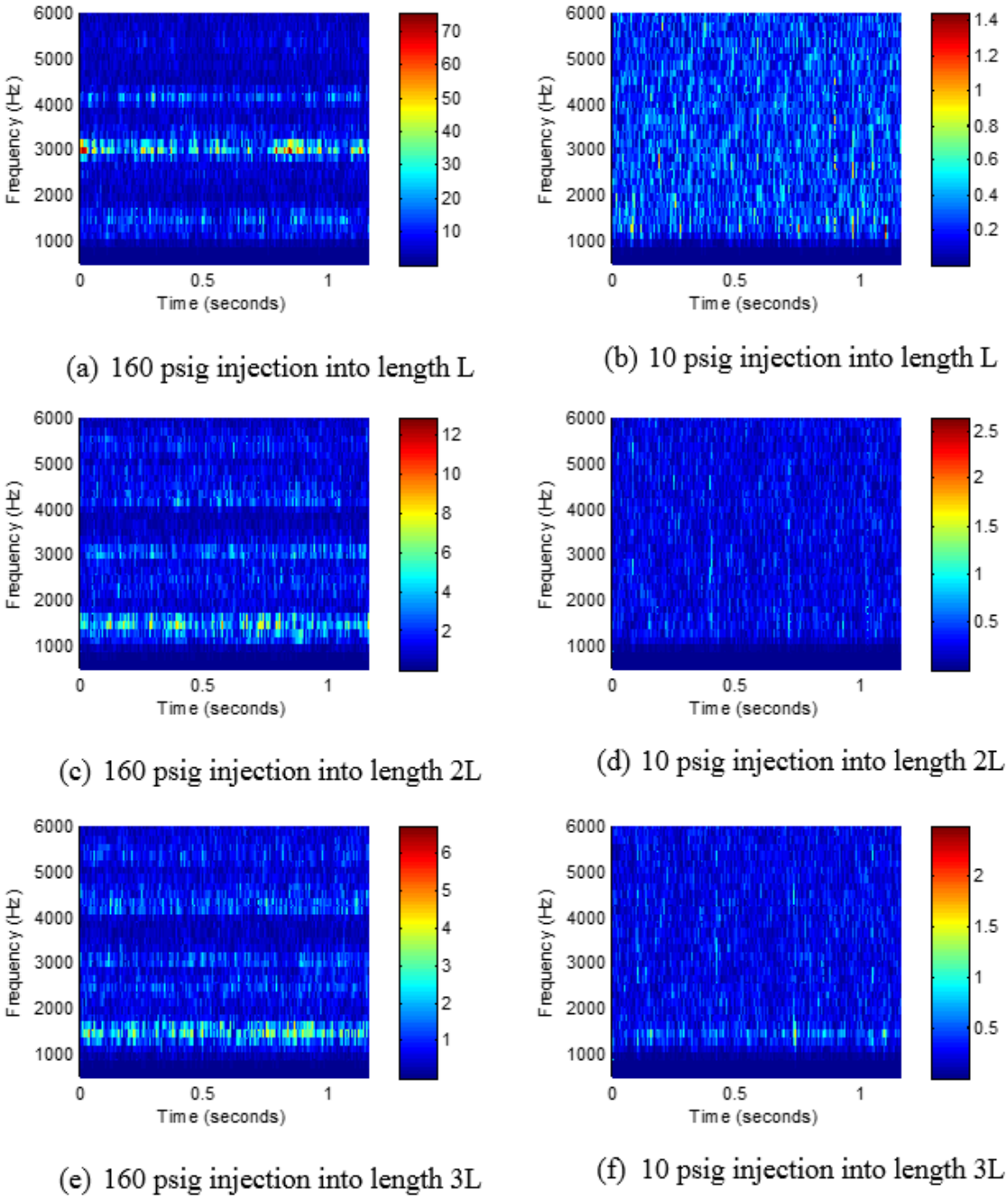

Fig. 37 STFT for Fluid Production from 30/50 Mesh Proppant

3.2 Effect of Fracture Length on Sound

3.2.1 20/40 Mesh

Calculating the sound pressure level for the frequency range between 1000 Hz to 6000 Hz, for each frequency spectrum obtained, we find that sound is related to the flow rate as shown in **Fig. 38**.

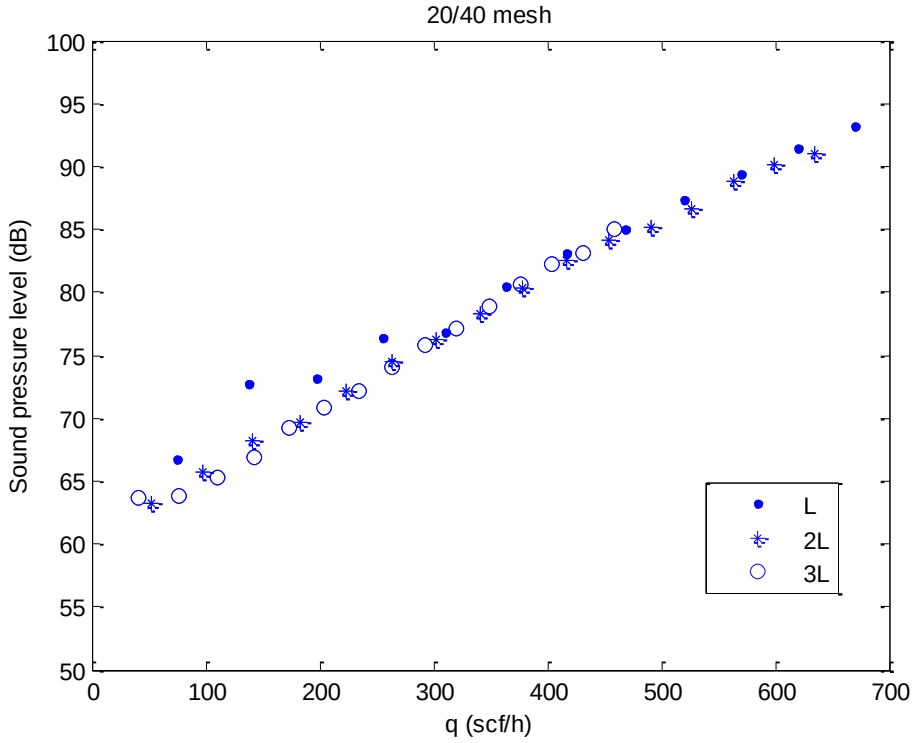

Fig. 38 Relationship between Production Rate and Sound Pressure Level for 20/40 Mesh Proppant

Each point on the plot represents an overall sound pressure level taken from 1000 Hz to 6000 Hz. As shown in **Fig. 38** the sound pressure level varies linearly with the

flow rate. This is true for the experiments where the proppant size was kept constant at 20/40 mesh and the fracture length was varied between 15 cm and 45 cm.

3.2.2 16/30 Mesh

Calculating the sound pressure level for the frequency range between 1000 Hz to 6000 Hz, for each frequency spectrum obtained with the 16/30 mesh experiments, we find that sound is related to the flow rate as shown in **Fig. 39**.

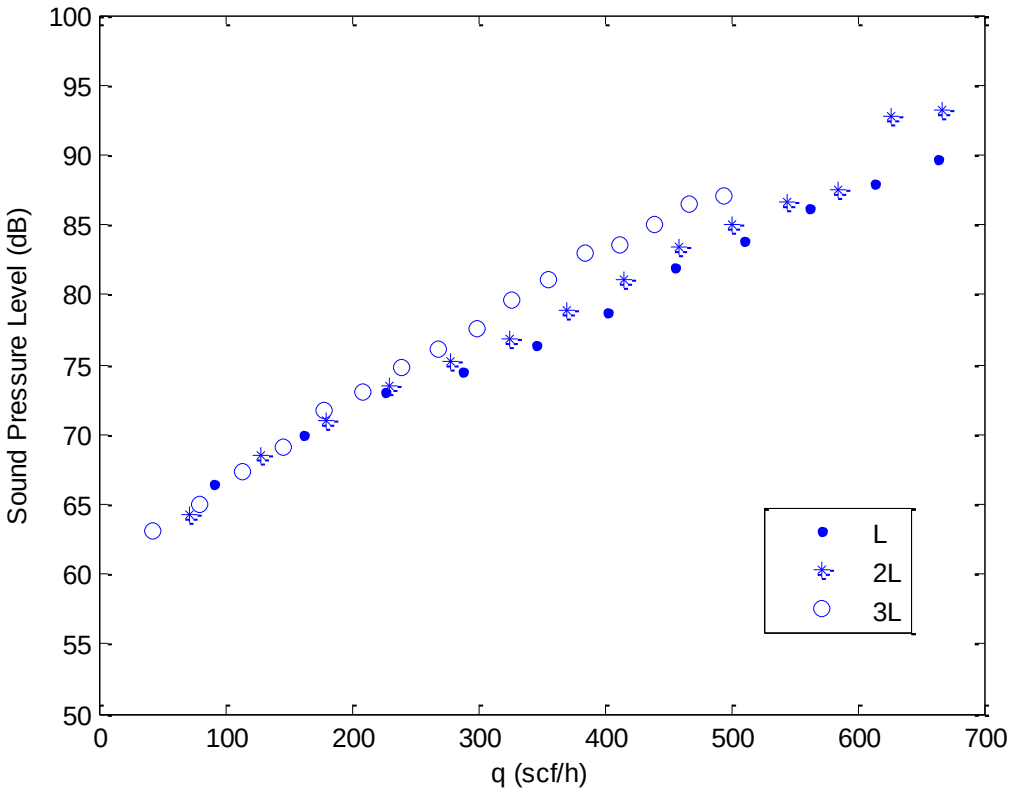

Fig. 39 Relationship between Production Rate and Sound Pressure Level for 16/30 Mesh Proppant

As stated in the previous section, each point on the plot represents an overall sound pressure level taken from 1000 Hz to 6000 Hz. In **Fig. 39** the sound pressure level varies linearly with the flow rate. This is true for the experiments where the proppant size was kept constant at 16/30 mesh and the fracture length was varied between 15 cm and 45 cm. It is noted that between 50 scf/hour and 300 scf/hour the trend is linear and at higher flow rates the curves begin to bend, indicating that the relationship between the flow rate and the sound pressure level may plateau at higher flow rates.

3.2.3 30/50 Mesh

Calculating the sound pressure level for the frequency range between 1000 Hz to 6000 Hz, for each frequency spectrum obtained with the 30/50 mesh experiments, we find that sound is related to the flow rate as shown in **Fig. 40**.

As stated in the previous two sections, each point on the plot represents an overall sound pressure level taken from 1000 Hz to 6000 Hz. In **Fig. 40** the sound pressure level varies linearly with the flow rate at rates above 100 scf/hour, however, the curves begin to bend as the flow rate increases. The point at which the curve begins to bend may be characteristic of the pressure gradient in the fracture. In addition, results from this experiments show that the sound generated at lower flow rates may be constant. This constant sound pressure level may be indicative of a lower bound to sound generated from fluid produced into a well.

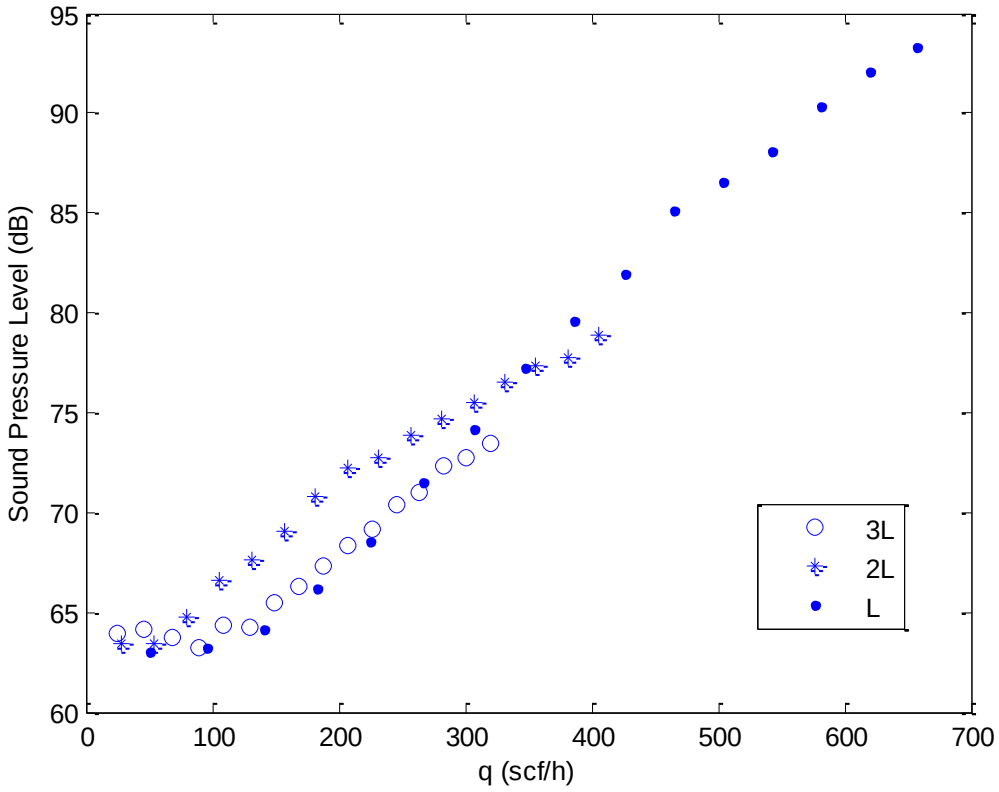

Fig. 40 Relationship between Production Rate and Sound Pressure Level for 30/50 Mesh Proppant

3.3 Effect of Proppant Size on Sound

Plotting the flow rates versus the sound pressure level for all proppant size experiments, we can see that the flow rate varies linearly with the sound pressure level. The results indicate that the proppant size does not overwhelmingly impact the sound that is being generated as a result of fluid being produced into a well from a proppant filled fracture. The plot is found in **Fig. 41**.

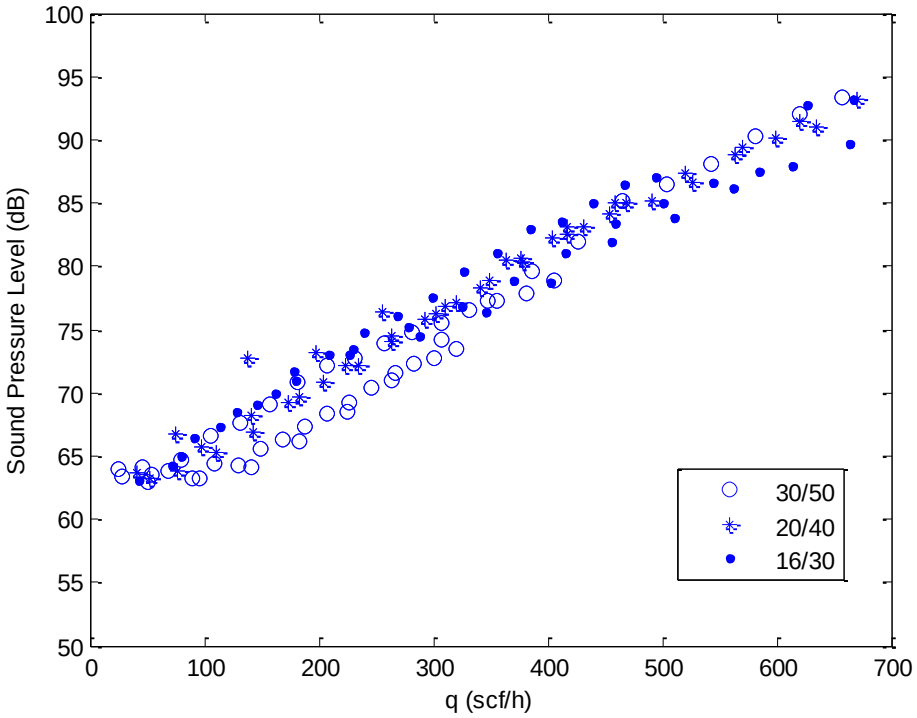

Fig. 41 Effect of Proppant Size on Generated Sound

3.4 Effect of Fracture Geometry on Sound

Calculating the sound pressure level for the frequency range between 1000 Hz to 6000 Hz, for each frequency spectrum obtained with different fracture-pipe diameters, we see that sound generated is affected by the dimension of the proppant filled fracture. This relationship is shown in **Fig. 42**.

The results in **Fig. 42** show that as the cross sectional area of the fracture decreases, the sound pressure level increases for a given flow rate. The sound pressure level for the 3/8 inch diameter fracture pipe is larger than that of the 2 inch because for the same flow rate the velocity of the fluid is larger in the 3/8 inch fracture than in the 2

inch fracture. These results indicate that as the velocity of the fluid increases so does the sound generated.

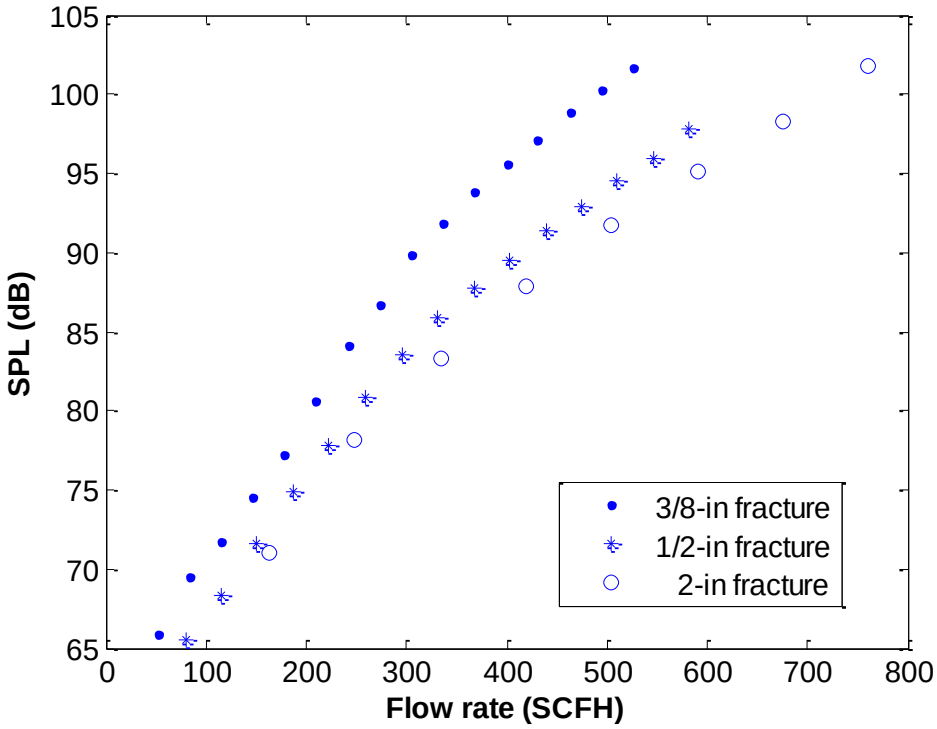

Fig. 42 Effect of Fracture Geometry on Sound

3.5 Discussion of Results and Limitations of Experiments

The results from the experiments indicate that sound from production is not influenced by the fracture length or proppant size but is solely impacted by the velocity of the fluid. This conclusion may be misleading because while the sound generated does not directly change with fracture length or conductivity, the flow of fluid which generates the sound does change with the fracture length and conductivity.

If we study how sound generated is affected by the flow power, we can make two observations (i) the sound pressure level approaches a steady value for all mesh sizes and in all fracture lengths with an increasing flow power (ii) sound pressure level increases with proppant size. These observations are made from **Fig. 43** where the sound pressure level is plotted against the flow power.

The trend of the curves indicates that a maximum sound pressure level will be reached with an increasing flow power. This maximum sound pressure level could be characteristic of the permeability and the dimensions of the fracture.

In addition, from **Fig. 43** it can be deduced that the sound pressure level increases with proppant size indicating that the larger proppants affect the transfer of energy from the flow to sound less. This is reasonable because as the permeability of the proppant pack increases so does the Reynolds number.

A limitation to this study is the shape of the simulated proppant filled fracture. In the experiments conducted, a pipe with a circular cross sectional area was used as a fracture. Fractures induced in formations have narrow widths as shown in **Fig. 44**. These narrow fractures are also confined by a closure stress. In the experiments conducted, the proppant in the pipes were not confined by a closure stress making the proppant pack very conductive. Due to the high conductivity of the proppant filled pipe, the length did not affect the sound generated as the largest pressure gradient occurs at the perforation and not along the length of the fracture.

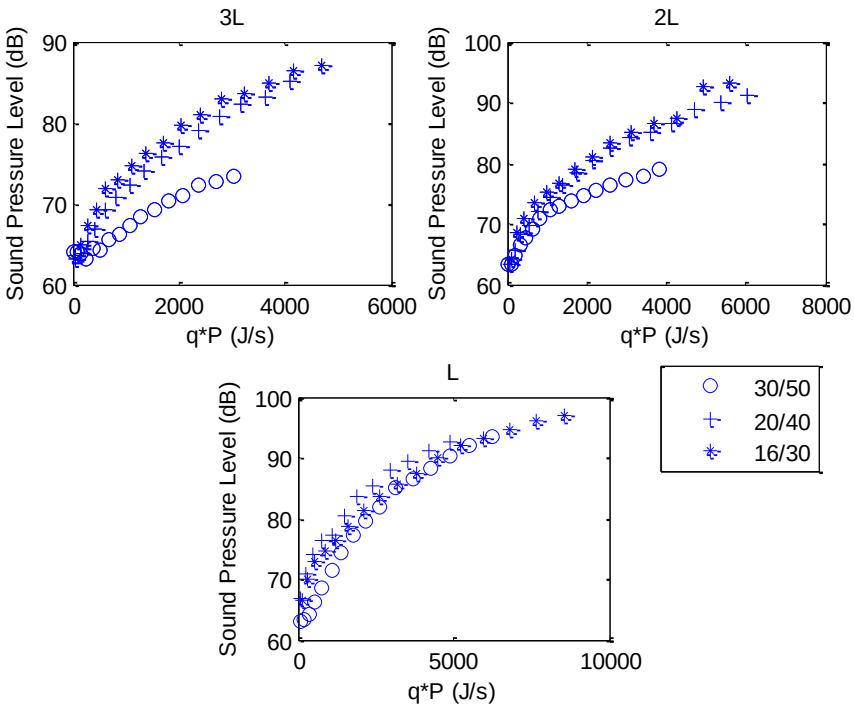

Fig. 43 Relationship between Sound Pressure Level and Flow power

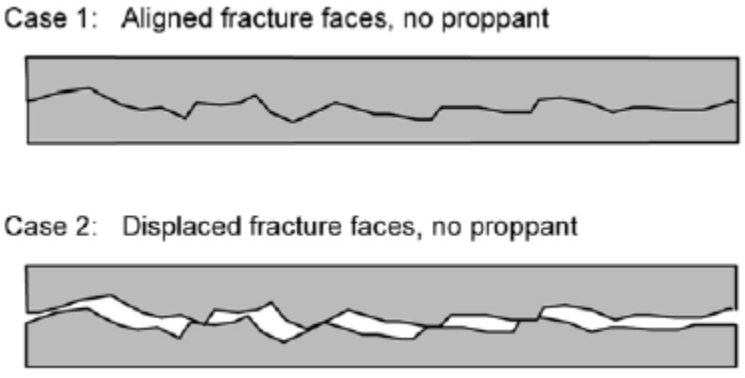

Fig. 44 Unpropped Fractures (Fredd et al. 2001)

4. RECOMMENDATIONS FOR FUTURE WORK

4.1 Modeling Sound Generation

Modeling sound generation will give insight into how fluid properties, velocity and pressure, influence sound that is being generated during hydraulic fracturing, fluid production and fluid leakage. The idea that sound can be simulated is not a new one. Aeroacoustic engineers have been interested in sound generated in flow fields such as in jet nozzle exhaust and mufflers, and have effectively modeled these sounds. Modeling sound generated by flow fields is known as computational aeroacoustics.

The objective of simulating sound would be to match the frequency spectrum obtained from experiments. If the simulated sound is matched with the sound recorded from the experiments then sensitivity studies can be conducted to understand how parameters such as perforation diameter, perforation tunnel length, fluid velocity, pressure gradient, fluid properties, and fracture dimensions affect sound that is being produced.

From these sensitivity studies, a forward model can be created to predict the sound that will be produced in an experiment given parameters such as, fluid density, velocity, pressure and perforation diameter and length. From this forward model, an inverse model is created to predict production rates from sound that is recorded.

Sound generation is modeled through a modification of Lighthills equation which relates sound to fluid flow parameters (Lyrintzis 2003). By coupling fluid flow

simulation and a sound generation model that takes the flow simulation results as inputs, sound generated in the experiments can be replicated.

4.1.1 Computational Aeroacoustics

There are two areas of focus in computational aeroacoustics that are relevant to simulating sounds in wellbores: (i) sound prediction tools, (ii) understanding of sound generation mechanisms (Hussaini 2011). The attempt to simulate the sound observed in experiments and in a wellbore will be an initial start to simulating sound in petroleum wells and can leave the two areas of focus to be further explored in the future.

A majority of jet noise prediction research is done with large-eddy simulation (LES) as it has shown promise in jet noise predictions (Uzun 2011). The commercial software, Ansys Fluent can be used to run an LES in which the perforation tunnel should be included as part of the computational domain

Sound computations are conducted by coupling time-accurate data provided from an LES and the Ffowcs Williams-Hawkings (FWH) method. The FWH method is implemented while the LES is running on the FWH surface, that is the surface that ecompasses the flow region in the perforation tunnel.

4.1.2 Large-eddy Simulation

Turbulence is a chaotic state of fluid motion that is observed when instabilities present in the initial or boundary conditions are amplified, and a self-sustained cycle is established in which turbulent eddies are generated and destroyed (Benocci 2004).The features of turbulent flow include: randomness, vorticity and mixing. LES is a

simulation in which only the large eddies are resolved by a filter, with the small scale appearing through a subgrid-scale (SGS) stress term.

In an LES the large and small scales are separated by filtering the flow variables f:

$$\bar{f}(x) = \int_D f(x')G(x,x')dx' \quad \text{..... (4.1)}$$

where D is the domain, G is the filter and the variable with the overbar is the filtered flow variable. A common filter function used is the Gaussian filter,

$$G(x) = \sqrt{\frac{6}{\pi\bar{\Delta}^2}}exp\left(-\frac{6x^2}{\bar{\Delta}^2}\right) \quad \text{..... (4.2)}$$

The filtered Navier-Stokes equations of motion can then be written in terms of the filtered variables:

$$\frac{\partial\overline{u_i}}{\partial x_i} = 0 \quad \text{..... (4.3)}$$

$$\frac{\partial\overline{u_i}}{\partial t} + \frac{\partial}{\partial x_j}\left(u_i u_j\right) = -\frac{1}{\rho}\frac{\partial\bar{p}}{\partial x_i} - \frac{\partial\tau_{ij}}{\partial x_j} + \vartheta\frac{\partial^2\overline{u_i}}{\partial x_i\partial x_j} \quad \text{..... (4.4)}$$

The small scale contributions is introduced into the LES through a subgrid-scale stress term,

$$\tau_{ij} = \overline{u_i u_j} - \overline{u_i}\,\overline{u_j} \quad \text{..... (4.5)}$$

By resolving the pressure, velocity and density of the fluid along the domain, we can simultaneously resolve the sound that is being generated from the fluid properties mentioned through the FWH method.

4.1.3 Ffowcs Williams and Hawkings Acoustic Analogy

In the simulation, the sound source is modeled with the Ffowcs Williams and Hawkings model, which is an inhomogenous wave equation derived by the manipulation of the continuity equation and Navier-Stokes equation. The FW-H equation is written as follows (Lyrintzis 2003):

$$\frac{1}{a_o^2}\frac{\partial^2 p'}{\partial t^2} - \nabla^2 p' = \frac{\partial^2}{\partial x_i \partial x_j}\{T_{ij}H(f)\} - \frac{\partial}{\partial x_i}\{[P_{ij}n_j + \rho u_i(u_n - v_n)]\delta(f)\} + \frac{\partial}{\partial t}\{[\rho_o v_n + \rho(u_n - v_n)]\delta(f)\} \quad \text{..... (4.6)}$$

where the terms on the right hand side are the source terms of sound generated,

$$\frac{\partial^2}{\partial x_i \partial x_j}\{T_{ij}H(f)\} = quadrupole\ noise \quad \text{..... (4.7)}$$

$$\frac{\partial}{\partial x_i}\{[P_{ij}n_j + \rho u_i(u_n - v_n)]\delta(f)\} = dipole\ noise \quad \text{..... (4.8)}$$

$$\frac{\partial}{\partial t}\{[\rho_o v_n + \rho(u_n - v_n)]\delta(f)\} = monopole\ noise \quad \text{..... (4.9)}$$

The solution to the above equation is found by using the free-space Green function. From this solution the surface integrals are source contributions from monopole and dipole, while the volume integrals are contributions from the quadrupole source. In FLUENT, the volume integrals are neglected and a solution to the above equation is found as (Lyrintzis, 2003):

$$p'(x,t) = p'_T(x,t) + p'_L(x,t) \quad \text{..... (4.10)}$$

where

$$4\pi p'_T(x,t) = \int_{f=0}\left[\frac{\rho_o(\dot{U}_n + U_n)}{r(1-M_r)^2}\right]dS + \int_{f=0}\left[\frac{\rho_o U_n\left(r\dot{M}_r + a_o(M_r - M^2)\right)}{r^2(1-M_r)^3}\right]dS \quad \text{..... (4.11)}$$

$$4\pi p'_L(x,t) =$$

$$\frac{1}{a_o}\int_{f=0}\left[\frac{\dot{L_r}}{r(1-M_r)^2}\right]dS + \int_{f=0}\left[\frac{L_r - L_M}{r^2(1-M_r)^2}\right]dS + \frac{1}{a_o}\int_{f=0}\left[\frac{\dot{L_r}\{rM_r + a_o(M_r - M^2)\}}{r^2(1-M_r)^3}\right]dS \quad \text{.....} \quad (4.12)$$

And the surface at f = 0 is thought of as a porous surface. As seen, the acoustic pressure terms are written in terms of the flow variables, and so can be resolved with the LES flow variables at multiple locations in the computational domain.

4.2 Experimental Set-up

A fracture cell that simulates a hydraulic fracture has been designed and built to replace the proppant-filled pipe in the experiments. The void which will hold proppant has a height of 10 inches and a length of 18 inches and width of 0.2 inches. The fracture cell will increase the convergence effect at the injection point in contrast to the proppant-filled pipe that is similar in size to the perforation tunnel. This convergence effect may give a more realistic empirical relationship between flow rates and sound generated. A picture of the fracture cell is found in **Fig. 45**.

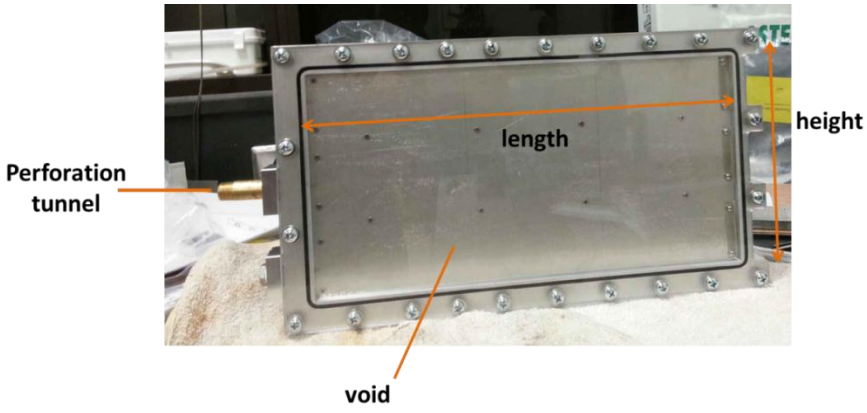

Fig. 45 New Fracture Cell

Conducting experiments with different diameters, lengths and roughness of the perforation tunnel will give an indication as to how the perforation tunnel affects sounds generated during production. In addition, building multiple fracture cells with different heights, lengths and widths will also give an insight into how the fracture geometry affects sound being generated.

This fracture cell has the ability to produce from multiple points. The cell can be connected to the well with up to three perforation tunnels. Conducting experiments with production from multiple points will require the use of multiple sensing points. By having multiple sensing points, the acoustic pressure inside the wellbore can be mapped. This mapping of the acoustic pressure in the well space, will be used to identify the fracture locations and to quantify the production from each perforation.

Once experiments are conducted with single phase gas flow, the next steps should include experiments with multiple phases. The following set of experiments would be ideal to conduct:

1. Inject water into the fracture cell and produce into the well
2. Fill the well with water and inject gas into the fracture and produce into the well
3. Inject water and gas into the fracture at varying volume fractions and produce into the well.

If the above experiments are successful, I suggest to repeat the mentioned experiments with an upwards flow in the well. More realistic sounds will be recorded during the experiments. The sound generated will need to be studied to make a

distinction between sound generated from fluid moving upwards in the well and fluid being produced from perforations.

5. SUMMARY AND CONCLUSIONS

The results from this study are from experiments conducted with a simulated hydraulically fractured well. Production from the simulated hydraulically fractured well was monitored with sound. One sensing point inside the well was used to measure sound generated from gas production. From these experimental results the following conclusions and observations were made:

1. Sound generated from production varies linearly in loudness with the flow rate.
2. The geometry of a fracture influences the sound that is generated. Sound generated from production is loudest in narrow fractures than in broader fractures.
3. The sound generation method in producing wells is due to the whistling phenomena.
4. There is a maximum and minimum sound pressure level generated when fluid is produced into a well.
5. The permeability limits the maximum sound pressure level observed in a well.
6. Further experiments where the geometry of the fracture and perforation tunnel vary, may give insight into how these parameters influence the sound generation.

REFERENCES

Benocci, C., 2006. Large Eddy Simulation and Related Techniques Theory and Applications. Rhode Saint Genèse.

Boone, K., Ridge, A., Crickmore, R. and Onen, D., 2014. Detecting Leaks in Abandoned Gas Wells with Fibre-Optic Distributed Acoustic Sensing, International Petroleum Technology Conference, Doha, Qatar.

Cannon, R., Aminzadeh, F., 2013. Distributed Acoustic Sensing: State of the Art, SPE Digital Energy Conference and Exhibition. Society of Petroleum Engineers, The Woodlands, Texas, USA.

Denn, M. M., 1980. Process Fluid Mechanics. Prentice-Hall, Englewood Cliffs, New Jersey.

Dranchuk, P.M. and Kassem, H.A.-. 1975. Calculation of Z Factors for Natural Gases Using Equations of State. Journal of Canadian Petroleum Technology, 14(3): 34-36.

Enright, R.J., 1955. Sleuth for Down-Hole Leaks. Oil and Gas Journal, 78-79.

Ferguson, S., 2002. Optical Fiber Technology: An Introduction to the Fundamentals. Intelligent Wells. Weatherford, (October): 4-6.

Fredd, C.N., McConnel, S.B., Boney, C.L. and England, K.W., 2001. Experimental Study of Fracture Conductivity for Water-Fracturing and Conventional Fracturing Applications. Society of Petroleum Engineers Journal, 6(3): 288-298.

Gonzalez, M.H., Eakin, B.E. and Lee, A.L., 1970. Viscosity of Natural Gases. Monograph on API Research Project 65. American Petroleum Institute, New York.

Hill, A.D., 1990. Production Logging: Theoretical and Interpretive Elements. Henry L. Doherty Memorial Fund of AIME, Society of Petroleum Engineers, Richardson, Texas.

Hussaini, M.Y. and Uzun, A., 2011. Prediction of Noise Generated by a Round Nozzle Jet Flow Using Computational Aeroacoustics. Journal of Computatinal Acoustics, 19(03): 291-316.

Lacombe, R., Foller, S., Jasor, G., Polifke, W., Auregan, Y. and Moussou, P., 2013. Identification of Aero-acoustic Scattering Matrices from Large Eddy Simulation: Application to Whistling Orifice in Duct. Journal of Sound and Vibration, 332(2013): 5059-5067.

Lyrintzis, A.S. 2003. Integral Acoustic Methods: From the (CFD) Near-field to the (Acoustic) Far-field. International Journal of Aeroacoustics, 2(2): 95–128

Martinez, R., Hill, A.D. and Zhu, D., 2014. Diagnosis of Fracture Flow Conditions with Acoustic Sensing, SPE Hydraulic Fracturing Technology Conference. Society of Petroleum Engineers, The Woodlands, Texas, USA Society of Petroleum Engineers.

Mateeva, A., Mestayer, J., Cox, B., Kiyashchenko, D., Wills, P., Lopez, J., Grandi, S., Hornman, K., Lumens, P., Franzen, A., Hill, D. and Roy, J., 2012. Advances in

Distributed Acoustic Sensing (DAS) for VSP, SEG Annual Meeting. Society of Exploration Geophysicists, Las Vegas, Nevada, USA.

McCain, W.D., 1990. The Properties of Petroleum Fluids, 2nd Edition. PennWell Publishing Company, Tulsa, Oklahoma.

McKinley, R.M., Bower, F.M. and Rumble, R.C. 1973. The Structure and Interpretation of Noise from Flow behind Cemented Casing. Journal of Petroleum Technology (March): 329-338.

Miller, C., Waters, G. and Rylander, E., 2011. Evaluation of Production Log Data from Horizontal Wells Drilled in Organic Shale. SPE North American Unconventional Gas Conference and Exhibition. Society of Petroleum Engineers, The Woodlands, Texas, USA.

Molenaar, M.M., Fidan, E. and Hill, D., 2012. Real-Time Downhole Monitoring Of Hydraulic Fracturing Treatments Using Fibre Optic Distributed Temperature and Acoustic Sensing, SPE/EAGE European Unconventional Resources Conference and Exhibition. Society of Petroleum Engineers, Vienna, Austria.

Molenaar, M. M., Hill, D., Webster, P., Fidan, E., & Birch, B., 2012. First Downhole Application of Distributed Acoustic Sensing for Hydraulic-Fracturing Monitoring and Diagnostics. SPE Drilling and Completion, 27(01): 32-38.

Poldervaart, L.J. Wijnands, A.P., Van Moll, L. and Van Voorthuisen, E.J., 1974. Modes of Vibration. Audio-Visual Center, Eindhoven University of Technology, The Netherlands.

Robinson, W.S., 1976. Field Results from the Noise-Logging Technique. Journal of Petroleum Technology, (November): 1370-1376.

Sutton, R.P., 1985. Compressibility Factors for High-Molecular-Weight Reservoir Gases, SPE Annual Technical Conference and Exhibition, Las Vegas, Nevada, USA.

Testud, P., Moussou, P., Hirschber, A. and Auregan, Y., 2007. Noise Generated by Cavitation Single-hole and Multi-hole Orifices in a Water Pipe. Journal of Fluids and Structures, 23(2): 163-189.

Testud, P., Auregan, Y., Moussou, P. The Whistling Potentiality of an Orifice in a Confined Flow using an Energetic Criterion. Journal of Sound and Vibration, 325(5): 769-780.

Van der Horst, J., Den Boer, H., Panhuis, P., Wyker, B., Kusters, R., Mustafina, D. and Green, K., 2014. Fibre Optic Sensing For Improved Wellbore Production Surveillance, International Petroleum Technology Conference, Doha, Qatar.

APPENDIX A

In this section, the correlations for the estimation of fluid properties used in this work are presented. **Table 4** summarizes the calculated fluid properties for two basins each producing gas with gas gravity of 0.61.

A.1 Gas Properties and Fluid Velocity

The fluid properties are calculated with the gas gravity, pressure and temperature of the reservoir gas.

A.1.1 Gas Compressibility Factor

Pseudo-critical pressure and temperature of natural gas are calculated with Sutton's equations (Sutton, 1985)

$$p_{pc} = 756.8 - 131.0\gamma_g - 3.6{\gamma_g}^2 \quad \text{..... (A.1)}$$

$$T_{pc} = 169.2 + 349.5\gamma_g - 74.0{\gamma_g}^2 \quad \text{..... (A.2)}$$

where the pseudo-critical pressure and pseudo-critical temperature are in psia and °R, respectively.

With the pseudo-critical pressure and temperature, the pseudo-reduced pressure and temperature are calculated by (McCain, 1990)

$$p_{pr} = \frac{p}{p_{pc}} \quad \text{.....(A.3)}$$

$$T_{pr} = \frac{T}{T_{pc}} \quad \text{.....(A.4)}$$

The gas compressibility factor is calculated with the expressions of Dranchuk and Kassem (1975)

$$z = 1 + \left(A_1 + \frac{A_2}{T_{pr}} + \frac{A_3}{{T_{pr}}^3} + \frac{A_4}{{T_{pr}}^4} + \frac{A_5}{{T_{pr}}^5}\right)\rho_{pr} + \left(A_6 + \frac{A_7}{T_{pr}} + \frac{A_8}{{T_{pr}}^2}\right){\rho_{pr}}^2$$

$$-A_9\left(\frac{A_7}{T_{pr}} + \frac{A_8}{{T_{pr}}^2}\right){\rho_{pr}}^5 + A_{10}\left(1 + A_{11}{\rho_{pr}}^2\right)\left(\frac{{\rho_{pr}}^2}{{T_{pr}}^3}\right)\exp\left(-A_{11}{\rho_{pr}}^2\right)$$

.....(A.5)

where

$$\rho_{pr} = 0.27\left[\frac{p_{pr}}{zT_{pr}}\right] \quad \text{.....(A.6)}$$

and $A_1 = 0.3265$, $A_2 = -1.0700$, $A_3 = -0.5339$, $A_4 = 0.05169$, $A_5 = -0.05165$, $A_6 = 0.5475$, $A_7 = -0.7361$, $A_8 = 0.1844$, $A_9 = 0.1056$, $A_{10} = 0.6134$, and $A_{11} = 0.7210$. This correlation applies under the following conditions

$0.2 \leq p_{pr} < 30$ for $1.0 < T_{pr} \leq 3.0$ .....(A.7)

$p_{pr} < 1.0$ for $0.7 < T_{pr} < 1.0$ .....(A.8)

A.1.1 Gas Density

Gas density is calculated by (McCain, 1990)

$$\rho = \frac{Mp}{zRT} \quad \text{.....(A.9)}$$

where

$$M = 28.97\gamma_g \quad \text{.....(A.10)}$$

$$R = 10.732\ \left[\frac{\text{psia}\cdot\text{ft}^3}{\text{lbmol}\cdot^\circ\text{R}}\right] \quad \text{.....(A.11)}$$

A.1.2 Gas Viscosity

The gas viscosity is estimated through the correlations presented by Gonzalez et al. (1970):

$$\mu_g = A(10^{-4})\exp(B\rho^C) \quad \text{.....(A.12)}$$

$$A = \frac{(9.379+0.01607M)T^{1.5}}{209.2+19.26M+T} \quad \text{.....(A.13)}$$

$$B = 3.448 + \frac{986.4}{T} + 0.01009M_a \quad \text{.....(A.14)}$$

$$C = 2.447 - 0.2224B \quad \text{.....(A.15)}$$

the unit of gas viscosity is in centipoises and *M* is given by Eq. (C.10).

A.1.3 Gas Formation Volume Factor

The gas formation volume factor is calculated by (McCain, 1990)

$$B_g = 0.0283\frac{zT}{P} \quad \text{.....(A.16)}$$

where the formation volume factor has units of (res ft^3/SCF).

Table 4 – Fluid Properties

Basin	Pressure [psia]	Temperature [°F]	B_g [res cf/scf]	ρ [lb/cf]	μ [cp]
Barnett	4000	205	0.0045	10.42	0.0222
Eagle Ford	6985	270	0.0034	13.88	0.0288

A.1.4 Gas Velocity

The gas velocity is dependent on the completions design in a well. For this study, the following completions assumptions are made: the well has 15 stages, 5 clusters per stage, each cluster is 2 ft and a peforation density of 5 shots per ft is assumed. From these assumptions, the number of shots can be calculated by

$$S_N = 15 \text{ stages} \times \frac{5 \text{ cluster}}{\text{stage}} \times \frac{2 \text{ ft}}{\text{cluster}} \times \frac{5 \text{ shots}}{\text{ft}} = 750 \text{ shots} \quad \text{(A.17)}$$

According to Miller et al. (2011), one third of perforation clusters are not contributing to production and in some basins, two thirds of production is coming from one third of the perforations.

The gas velocity at reservoir conditions can be calculated by

$$v = \frac{B_g Q_t}{S_N \times A_p} \quad \text{(A.18)}$$

where Q_t is the total production in scf, A_p is the perforation cross-sectional area in ft^2. If the perforation diameter is assumed to be 0.3 inches and that one third of perforation clusters are not contributing to production, the fluid velocity through the perforation can be estimated. **Table 5** reports the fluid velocities through perforations at reservoir pressures and temperatures stated in **Table 4**.

Table 5 – Fluid Velocity through a Perforation

Basin	Q [MMSCF/D]	Active Perforations	Velocity [m/s]
Barnett	10	500	2.11
Eagle Ford	10	500	1.58

A.1.5 Reynolds Number

The Reynolds number is calculated by

$$N_{Re} = \frac{\rho v D}{\mu} \quad \text{..... (A.19)}$$

The Reynolds number for the Barnett and Eagle Ford basin gas wells each producing 10 MMSCSF/day at the temperature and pressure stated in **Table 4** are presented in **Table 6**.

Table 6 – Reynolds Number

Basin	ρ [lb/cf]	μ [cp]	v [m/s]	D [in]	N_{Re}
Barnett	10.42	0.0222	2.11	0.3	3423
Eagle Ford	13.88	0.0288	1.58	0.3	2634

APPENDIX B

B.1 MATLAB Code

```
clear all ; clc
SPL_all=[]; % initiate array for sound pressure level
for  n=1:16 %

    if n==1
        filename='30_50_L_160.xlsx'

    end

    if n==2
        filename='30_50_L_10.xlsx'

    end

    if n==3
        filename='20_40_2L_140.xlsx'
    end

    if n==4
        filename='20_40_2L_130.xlsx'
    end

    if n==5
        filename='20_40_2L_120.xlsx'
    end

    if n==6
        filename='20_40_2L_110.xlsx'
    end

    if n==7
        filename='20_40_2L_100.xlsx'
    end

    if n==8
        filename='20_40_2L_90.xlsx'
    end

    if n==9
        filename='20_40_2L_80.xlsx'
    end
    if n==10
        filename='20_40_2L_70.xlsx'
    end

    if n==11
```

```
        filename='20_40_2L_60.xlsx'
    end

    if n==12
        filename='20_40_2L_50.xlsx'
    end

    if n==13
        filename='20_40_2L_40.xlsx'
    end

    if n==14
        filename='20_40_2L_30.xlsx'
    end

    if n==15
        filename='20_40_2L_20.xlsx'
    end

    if n==16
        filename='20_40_2L_10.xlsx'
    end

sheet=2; % sheet number in excel file
tRange='A2:A25601'; % range of time
amplitudeRange='B2:B25601'; % range of amplitudes
time = xlsread(filename, sheet, tRange); % uploads time data
amplitude= xlsread(filename, sheet, amplitudeRange);
charge_amp=0.0316; % charge amplification
amplitude=amplitude/charge_amp;


Fs=22*10^3; % sampling frequency in Hz


% filter
[B,A]=butter(10,.1,'high'); % initiates high pass filter
d=filter(B,A, amplitude); % applies high pass filter
[B,A]=butter(10,.7, 'low'); % initiates low pass filter
d=filter(B,A, d); % applies low pass filter


L=Fs; %

% fourier transform
NFFT=2^nextpow2(L);
H=fft(d, NFFT)/L;
f=Fs/2*linspace(0,1,NFFT/2+1);

SPL=10*log10(sum((abs(H(1:NFFT/2+1))).^2)/((20*10^-6)^2)) % calculate
overall sound pressure level
```

```
SPL_all=[SPL_all SPL];   % store overall sound pressure level


figure(n) % plot frequency spectrum
plot(f, abs(H(1:NFFT/2+1)));
set(gca, 'YTickLabel', num2str(get(gca, 'YTick')'))
xlim([0 6000])
hold on
xlabel('Frequency (Hz)')
ylabel('Amplitude (Pa)')


% plot STFT
figure(16+n)
% subplot(1,2,2)
[B,fg,t]=spectrogram(d,130,[],130,Fs);
mesh(t,fg,(abs(B))); hold on;
xlabel('Time (S)')
ylabel('Frequency (Hz)')
axis([0 times 500 6000])
% caxis([40 120])
 set(gca,'YDir','Reverse')

end
```